LONGSHORE MIGRATTION OF SHORELINE MEGA-CUSPS OBSERVED WITH X-BAND RADAR

Elsayed M. Galal[1*] and Satoshi Takewaka[2]

Department of Engineering Mechanics and Energy

Graduate School of Systems and Information Engineering

University of Tsukuba, Tsukuba, Ibaraki, 305-8573, Japan

[1]*sayed@surface.kz.tsukuba.ac.jp*

[2]*takewaka@kz.tsukuba.ac.jp*

Fax: +81-029-853-5207

[*]*Corresponding author*

Abstract

Intertidal morphology was monitored continuously with an X-band radar at the research pier HORS in Hasaki, Japan. Hourly-averaged radar images were processed to observe longshore distributions of shoreline positions. Variations of longshore mean shoreline positions and their fluctuation intensities observed in the years 2005 and 2006 showed a seasonal change which followed the so-called beach-cycle. Longshore pixel intensities close to the waterline were extracted from time-averaged images for every hour of the two years to process longshore time-stack image. Longshore migration speeds of shoreline mega-cusps were estimated by cross correlation analysis of the time-stack image, and the reliability of the method was checked. Migration speeds were compared to measured longshore current speeds at the pier and the longshore component of the wave power, showing that they are highly synchronized for most conditions. Finally, the migration statistics were related to the wave data, and the results showed that the northwards migration rates were typically larger than southwards rates, which was consistent with the statistical results for wave forcing variables. Also, the relationship between the migration speeds and the forcing variables indicates that the migration was more active when the wave incidence angle was close to 45°.

Keywords: X-band radar; longshore migration; intertidal morphology; cross correlation; shoreline positions.

1. Introduction

1.1 *Aim of the study*

Longshore migrations of coastal features, such as shoreline, foreshore morphology, transverse bars, bar system, and rip channels, are observed on coasts all over the world and are fascinating for scientists and annoying for engineers. This paper displays the results of continuous X-band radar observation of a shoreline within the intertidal region through the years 2005 and 2006 on the Hasaki Coast, Japan, facing the Pacific Ocean. The objective of the work is to estimate the longshore migration speeds of shoreline mega-cusps from radar images. The results are compared with longshore current velocities observed at the site and the longshore component of the offshore wave power. Finally, the link between the migration speeds and the wave state are discussed.

1.2 *Pervious studies*

Long sandy coasts commonly show longshore periodicities that have a range of spatial, and corresponding temporal scales. Shoreline beach cusps [Sallenger, 1979; Komar, 1971], transverse bars [Bruner and Smosna, 1989; Konicki and Holman, 2000], ridges and runnels [De Melo Apoluceno et al., 2002; Lafon et al., 2004, 2005], and crescentic bars [Wright and Short, 1984; Van Enckevort and Ruessink, 2003; Van Enckevort et al., 2004] are examples of these particular features. Sand beaches are seldom straight, but rather commonly contain

crescentic seaward projections, sometimes isolated but more often in a rhythmic series with a fairly uniform spacing. The shoreline of Hasaki is consistently characterized by undulating shoreline features that would be locally referred to as longshore shoreline “mega-cusps” or “giant-cusps” or “sandwaves”. These features have longshore scales on the order of 10^2-10^3 meters and a temporal scale of days to months. These rhythmic features generally occur on coasts with a high net rate of longshore sediment transport and characterized by seaward protruding accretion horns and erosive embayment cusps associated with rip currents, as shown in Fig. 1. The shoreline features discussed in this paper are distinguished from commonly observed beach cusps, which have longshore scales of 10^1 meters and a temporal scale of hours to a few days [Sallenger, 1979], since the shoreline undulations found on Hasaki appear to be more random with respect to their spatial distribution and have wavelengths that are substantially longer than those of beach cusps.

The features that are the focus of this study have had limited study, despite being identified early in the field of coastal processes. These features have acquired the descriptive names "sand waves" and "shoreline rhythms" [Bruun, 1954; Dolan, 1971]. Shepard [1952] classifies them as “giant cusps.” Dolan [1971] contains particularly excellent examples from the North Carolina coast that occur as either rhythmic or independent forms and they generally have a longshore length scale on the order of hundreds of meters, similar to sand waves, arrhythmic giant cusps, and rhythmic giant cusps. Such features are therefore

considerably larger than "beach cusps" as that term is generally applied. Observations by Komar [1971] in the field and the laboratory indicated that rips emerged from the shoals. This result is consistent with the relationship between breaking wave height and depth; i.e., rhythmic bathymetric contours in the nearshore force rips from embayments into shoals. Wright [1980], Short and Hesp [1982] and others observed that erosion of intermediate beaches are dominated by the presence of rip currents, with maximum erosion occurring in the lee of the rip current creating a mega-cusp embayment. The shoreline circulation is usually accompanied by bed forms in the inner surf zone which are in phase with the crescentic bars, and these features could be related to mega-cusps observed on natural beaches and reported by Wright and Short, [1984]. Calvete et al. [2005] found, by using a morphodynamic stability model, that there was a rip circulation cell close to the shoreline that was more prominent for low energy conditions and caused mega-cusps-like bed forms in phase with the crescentic bar morphology, horns in front of the shoals, and embayments in front of the rip channels. Recently, Thornton et al. [2007] found that the longshore variations of the shoreline mega-cusps were significantly correlated with the longshore variations in rip spacing. Dalon [2007] reported that rip embayments appear to be distributed randomly along the coastline with no correlation in the locations from year to year. However, there does appear to be a correlation between the location of the embayments and the local slope in the cross-shore profile, with the slope tending to reach a maximum at the center of the

embayment.

Longshore processes remain less explored because ordinary survey methods lack sufficient longshore coverage. However, longshore migration of nearshore rhythmic patterns, such as shoreline, foreshore morphology, transverse bars, bar system, and rip channels, is evidenced in topographic and video imagery. Table 1 presents some of the few examples available of previous observations of the migration of these features. Bathymetric surveys, cross-shore profiles and video-based observations are commonly investigated to detail the longshore behavior of coastal features and are admittedly precise. In particular, video monitoring presents the possibility of frequently repeated observations on a long-term time scale. However these techniques provide only restrictive survey coverage and thus allow study of just a few number of features at a time. Alternatively, high-resolution satellite imagery and frequently constructed, detailed maps of wide areas have proven particularly successful in characterizing nearshore beach morphodynamics and coastline changes.

X-band marine radar is an imaging radar that is capable of tracking the movements of wave crests over an area spanning several kilometers, and is becoming popular in coastal studies these days. The most attractive feature of using an X-band radar system is its ability to collect data on coastal processes, continuously and remotely, in bad weather through moderate levels of fog and rain that typically accompany erosive high-wave conditions. X-Band radar research significantly advanced in the 1980s. Young et al. [1985] first described an approach

using a three-dimensional Fourier transform analysis on a sequence of radar images to calculate wave lengths and periods, providing an accurate estimation of ocean wave properties. Further developments in technology allowed researchers to start digitally recording data directly from the radar in the 1990s. Bell [1999, 2001] succeeded in determining near-shore bathymetry after analyzing X-band radar images. Borge and Soares [2000] estimated the wave spectra of wind waves and swells along the Spanish coast. Ruessink et al. [2002] reported on the detection of coastal bars using time-averaged radar images. Takewaka and Nishimura [2005] analyzed radar images for run-up analyses during a storm. Takewaka [2005] also analyzed time-averaged X-band radar images to quantify shoreline position and intertidal foreshore slopes; Hasan and Takewaka [2007] described the general applicability of X-band radar observations to energetic sea state and succeeded in estimating hydrodynamic parameters during a typhoon event. Esteves et al. [2007] examined temporal and spatial changes in nearshore morphology using time-averaged images obtained by X-band radar along the beach, while Jesse E. McNinch [2007] used a mobile X-band radar to construct maps of the shoreline and nearshore sand bars that exhibited high correlation with Argus video data and bathymetric profiles. This paper shows an application of radar image data for visualizing the temporal and spatial characteristics of a shoreline's wavy pattern "mega-cusps" migration.

Figure: 1

Table: 1

2. Field Experimental

2.1 *Set-up*

X-band radar measurements were conducted at the research pier of the Hasaki Oceanographic Research Station (HORS) of the Port and Airport Research Institute (PARI), located in Hasaki, Japan, as shown in Fig. 2. The main facilities are a 400 m length pier extending into the Pacific Ocean and a research building located nearly 110 m backward from the mean shoreline position. HORS is on an almost straight sandy coast approximately 17 km long with Choshi Fishery Port at the south end and Kashima Port at the north end of the coast. The pier is located approximately 4 km from Kashima Port. Bottom profile and longshore velocities along the pier are surveyed on weekdays. The x-axis corresponds to the long-shore extent and directs positive towards Choshi Fishery Port and the y-axis coinciding with the pier and oriented in the offshore direction (Fig. 2 and Fig. 3). Along Hasaki beach, the median sediment diameter is 0.18 mm and almost uniform, but occasionally increases to 1.0 mm around troughs after extreme storms [Katoh and Yanagishima, 1995]. Hasaki coast basically has a single bar and a mean beach slope of 1/50 from -60 m to 200 m seaward and 1/20 in deeper region [Kuriyama, 2002].

Figure: 2

2.2 *Wave and tide data*

Offshore waves are measured by the Nationwide Ocean Wave Information Network for Ports

and Harbors (NOWPHAS; http://nowphas.mlit.go.jp/eng.html) station at Kashima Port, where the mean water depth is approximately 24 m. Significant offshore wave height $H_{1/3}$, wave period $T_{1/3}$, and wave propagation angle $\theta_{1/3}$, are measured every 2 hours. The wave angle in this study is defined as the angle measured counter-clockwise from the shoreline, as shown in Fig. 2. The tide level is measured every hour by the Japanese Meteorological Agency at Choshi Fishery Port approximately 13 km south of HORS.

2.3 *Radar system*

The radar system employed in this study is a conventional marine X-band radar, usually installed on fishing or recreational boats. The radar antenna is installed on the roof of the research building 17 m above the mean sea level. The antenna rotates with a period of approximately 2.5 s and transmits with a beam width of 0.8° horizontally and 25.0° vertically. The echo signals from the sea surface, generally called sea clutter, are captured with a specially designed A/D board installed on a computer. The echo signal over sampled at every 2-second intervals and part of the image is not renewed since the imaging intervals are shorter than the rotation time of the antenna. The echo signal is stored as an image comprised of 1024 x 512 pixels with 8-bit numerical resolution and each pixel corresponds to 5.4 m x 5.4 m spatial resolution. For the details, refer Takewaka [2005] and Hasan and Takewaka [2007].

2.4 *Time-averaged image*

Individual echo images sampled every 2 seconds were averaged yielding a "time-averaged image" or so-called "time-exposure". The system grabs 512 echo images (512 x 2 sec = 1024 sec) from 0 to 17 minutes of every hour. The sequence of images is analyzed for other studies on wave motions [Hasan and Takewaka, 2007]. Fig. 3 shows images averaged over 17 minutes for a complicated shoreline and bar system observed during a calm sea state and a straighten condition during a stormy state. The horizontal extent of an image is 5556 m (3.0 nautical miles). Individual waves disappear in the time-averaged image and an edge extending in the long-shore direction becomes visible. Several features, such as the breaker zone, shoreline position, and bar crest locations, can be estimated using the averaged image. The accuracy of intertidal morphology mapping with averaged images has been examined with survey results by Takewaka [2005]. Time-averaged images have been processed hourly and accumulated from the year 2004 to the present except for some lapses due to system trouble.

Figure: 3

3. Beach Morphology: Overall State

3.1 *Wave and tide record for 2005 and 2006*

Variations of tide levels and offshore significant wave incidence angle $\theta_{1/3}$, significant wave period $T_{1/3}$, and significant wave height $H_{1/3}$ in 2005 and 2006 are shown in Fig. 4. Tide levels are converted to Datum Level (D. L.), where D.L. 0 m is 0.687 m below the mean sea level of

Tokyo Bay (Tokyo Peil, T.P.).

Energetic events during the study period were identified when maximum wave height $H_{1/3}$ exceeded 3.5 m. The duration of an energetic event was defined as the period over which the hourly significant wave height remained higher than 3.0 m, starting immediately before and finishing immediately after the energetic event peak. If there were several consecutive events, they were considered as one single event if the time gap between them was less than or equal to 12 hours. Table 2 displays the date, peak wave height $H_{1/3}$, its period $T_{1/3}$, angle $\theta_{1/3}$, and the duration of the 18 energetic events that were observed during the two-year study.

Figure: 4

Table: 2

3.2 *Mean shoreline locations and their longshore variability*

Shoreline positions $Y_s(t, x)$ at longshore position x and time t were digitized manually when the tide level measured at the Chosi Fishery Port was between 0.75 m and 0.85 m (local D.L.), which are the most frequent tide levels observed at the site. 541 time-averaged images met this condition during 2005 and 2006. The accuracy of the shoreline digitization has been confirmed by Takewaka [2005] by comparing survey results around the pier and radar estimation.

Longshore mean shoreline position $\overline{Y}_S(t)$ at t is defined as

$$\overline{Y}_S(t) = \frac{1}{x_1 - x_0} \int_{x_0}^{x_1} Y_S(t, x)\, dx \qquad (1)$$

and the fluctuation intensity $Y'_S(t)$ at t as

$$Y'_S(t) = \sqrt{\frac{1}{x_1 - x_0} \int_{x_0}^{x_1} \left(Y_S(t,x) - \overline{Y}_S(t) \right)^2} \qquad (2)$$

where, x_0 = -2727 m and x_1 = 2829 m are the limits of the imaging extent.

Fig. 5 displays seasonal variations of longshore mean shoreline positions $\overline{Y}_S$ and fluctuation intensities Y'_S observed in 2005 and 2006. Macroscopic variations of the mean shoreline position $\overline{Y}_S$ are seaward shifts during the periods from April to September, and landward shifts during the following period. The mean shoreline position $\overline{Y}_S$ showed quick recessions, and the fluctuation intensity Y'_S decreased suddenly due to the energetic events defined in Table 2. Generally speaking, during seaward shifts of the mean shoreline position $\overline{Y}_S$, the intensity of the fluctuation Y'_S increases and vice versa for the retreat of the shoreline.

The features observed in the mean shoreline positions match well the results reported by Kuriyama and Lee [2001] who analyzed the daily bathymetric data measured along the pier and described the seasonal behavior of the beach. The changes observed here are parts of the so-called beach-cycle proposed by Wright and Short [1984].

Figure: 5

4. Observations of Longshore Shoreline Mega-Cusps

4.1 *Mega-cusps formation and decay*

The shoreline of Hasaki is consistently characterized by undulating shoreline features that have longshore scales on the order of 10^2-10^3 meters and a temporal scale of days to months. Shoreline mega-cusps formation, stability, and decay were observed in relation to several factors, including tidal range, wave height and period, behavior of incident waves, shore slope, size of sediment, storm events and frequencies, and the preexisting morphology.

Beach cusps gradually develop non-uniformities (wavy patterns) during low-wave conditions whereas the development of rhythmic patterns is typically sequential with increasing longshore variability over time and after that it remains stable at relatively fixed longshore wavelengths until a storm event occurres, which destroys the cusp pattern. Fig. 6 shows a time sequence of time-averaged radar images observed at the same tide level between 0.75 m and 0.85 m (local Datum Level) which were captured between two energetic events, number 16 and 17 in Table 1. These images show the evolution of shoreline features during this period. The shoreline and bar were straightened during the high energy event number 16 and after 4 - 5 days the system began to show some perturbations. Later, the system began to develop rip channels, and in front of the rip channels mega-cusps developed embayments and horns in front of the shoals. After that, the system remained stable at relatively fixed longshore wavelengths until the next event (number 17) occurred and the system became uniformed longshore.

Figure: 6

4.2 *Longshore migrations of shoreline mega-cusps*

In the sequence of time-averaged radar images, we observed longshore movement of shoreline mega-cusps within the intertidal region. Examples of migrations are shown in Fig. 7, which displays digitized shoreline positions and corresponding time-averaged images. Fig. 7 (a) shows an example of a time history of shorelines digitized for the period of 3rd February to 10th February 2005, while Fig. 7 (b) shows a time history of shorelines digitized for 7th November to 13th November 2006. Fig. 7 (a) indicates that there is a migration of the shoreline mega-cusps longshore towards the positive direction (+x) with an approximate migration speed of 18 m/day. On the other hand, Fig.7 (b) indicates that the mega-cusps migrate towards the negative direction (-x) with a speed of 9 m/day.

Migration speed and direction are highly variable and also the scale of the mega-cusps. In the following, temporal and spatial behaviors of migrations are visualized to gain a better understanding of their nature.

Figure: 7

4.3 *Visualization of longshore migration of shoreline mega-cusps using longshore time-stack*

To visualize the temporal and spatial variation of the migration, time-stack images were processed. A time-stack image is a composite image with one axis representing time, and the

other, the coastal extent. Longshore pixel intensities close to the waterline were extracted from time-averaged images for each hour as explained in Fig. 8. Cross-shore locations of the extractions have been shifted from the mean position in accordance with tide level variation. They have been shifted onshore wards for high tides and off-shore wards for low tides. The amount of shift has been determined empirically from tidal variation and foreshore slope.

The results are shown in the main panel of Fig. 9 with the observed significant wave height and wave angle by NOWPHAS indicated in the right panels. The horizontal extent of the main panel is the longshore extent and the vertical is the elapsed time from January 2005 to December 2006. Black-white patterns in the diagram show the locations of waterlines and dried areas with seawater bright and dried shore dark. The vertical bright streak in the diagram is the pier. There are several missing periods due to system trouble which are represented as horizontal black regions in the time-stack image. In the diagram, the 18 energetic events listed in Table 1 are also depicted with numbers and arrows.

Oblique patterns or streaks are observed in the diagram. They extend to the lower right mostly in January, February and December- the winter months- and to the lower left in the other months. This indicates that shoreline mega-cusps observed in the intertidal morphologies are migrating in the direction of the streaks and with speeds proportional to the slope of the streaks. Oblique patterns become blurred when high waves attack the shore, for example at the end of July 2005. The coast is straightened in stormy periods, as described

previously. Consequently, the longshore variation of pixel intensities becomes small and the coast appears as bright uniform strips in the time-stack image. The featureless part between the storm event 5 and 6 in the main panel of Fig.9 corresponds to low fluctuation intensity period of Y'_S, which means that the shore was rather uniform. The slope of the oblique patterns is analyzed in the next section.

Figure: 8

Figure: 9

5. Estimation of Longshore Migration Speeds of the Observed Mega-Cusps

In this section, the longshore migration speeds of shoreline mega-cusps for the entire study period are estimated by cross correlation analysis of the time-stack image. First reliability of the method is checked. After that, the estimated results of the migration speeds are compared with the field measurements of longshore current speed at the pier. Finally, the migration statistics are discussed in relation to the wave data.

Before applying the cross correlation analysis, we excluded the region close to the pier where echo signals were saturated, and the domain was divided into two parts. x = -2727 and x = -70 m are the starting and ending boundaries of the first domain, and x = 162 m and x = 2829 m are those for the second domain as shown in Fig. 10. This diagram shows longshore pixel-intensity distribution for two different hours extracted from time-stack image (shown in Fig. 9) which depicts that pixel-intensity has higher values close to the radar position. The reduction of intensity observed in the longshore is due to increase of travel distances of the

electro magnetic rays emitted from the radar antenna.

Figure: 10

5.1 *Cross-correlation analysis method*

Migration speeds of mega-cusps were estimated by cross correlation analysis of two longshore pixel-intensity distributions in time-stack image 24 hours apart. First, the pixel intensity distribution $f(t, x)$, where f is the pixel intensity at longshore position x and time t, was linearly de-trended yielding $f'(t, x)$ as shown in Fig. 10. Then, cross correlation analysis was applied to $f'(t, x)$ and $f'(t+\Delta t, x)$:

$$r(t, \Delta x) = \frac{\int_{x_{co}}^{x_{c1}} f'(t, x) * f'(t + \Delta t, x + \Delta x)\, dx}{\sqrt{\int_{x_{co}}^{x_{c1}} f'(t, x)^2\, dx} * \sqrt{\int_{x_{co}}^{x_{c1}} f'(t + \Delta t, x + \Delta x)^2\, dx}} \quad (3)$$

Here, r is the cross correlation coefficient at time t and longshore displacement Δx. The values of the starting and ending limits of the template used in cross correlation in each domain are; x_{co} = 352 m and x_{c1} = 2639 m are for the first domain and x_{co} = -260 m and x_{c1} = -2537 m are those for the second domain. Migration speeds of the shoreline mega-cusps were determined from the displacement Δx which gave the maximum cross correlation r and the migration speed was determined as

$$V = \frac{\Delta x}{\Delta t} \quad (4)$$

Positive (negative) displacement corresponds to southward (northward) migration. Δt is the time step between two pixel-intensity distributions, 24 hours in this study. Fig. 11 is a schematic showing the definition of different variables used in the cross-correlation analysis.

There were several considerations associated with the analyses that had to be taken into account when estimating the migration speeds. These included gaps in the image data set due to missing measurements, high energy events, and outliers in the correlation's results. There were several time periods within the two-year study period for which no images were available due to system failure. Most of these periods occurred before April 2005, so the analyses start from the 11th of April 2005; however, other periods after this time were excluded from the analyses, such as the end of July 2006. Also, if the waves were high on a given day, which straightened the coast, it was impossible to discern features from the pixel intensities so these days were excluded from the analysis. Finally, we sometimes observed extreme values for the longshore displacement Δx, so a manual inspection of the results was done to exclude these non-realistic results. *Figure: 11*

5.2 *Method validation*

In order to validate the accuracy of the analysis, shoreline positions Y_{SC} *(t, x)* at longshore position *x* and time *t* were digitized manually for the period between 15th June 2006 to 25th

July 2006. Shoreline positions were digitized from time-averaged radar images at every hour, yielding 974 shoreline data sets. The deviation of the shoreline position Y'_{SC} *(t, x)* from the mean $\overline{Y}_{SC}$ *(t)* is defined as follows:

$$Y'_{SC}(t,x) = Y_{SC}(t,x) - \overline{Y}_{SC}(t) \tag{5}$$

Distributions of Y'_{SC} *(t, x)* are displayed as a time-stack in the right panel of Fig.12. The deviation lines are vertically stacked with dark (light) colors corresponding to seaward (landward) deviations. Thus, the mega-cusps are displayed as a horizontal alternation of dark and light colors. Longshore migration is reflected by a vertical displacement in the location of the color bands. A time-stack of longshore pixel intensities from radar images for the same period is displayed in the left panel of Fig. 12. Both time-space diagrams indicate oblique patterns or streaks extending from the upper right to lower left.

Cross-correlation analysis was applied to Y'_{SC} and pixel intensity time-stacks to compare the migration speeds V'_{SC} and V_{SP}. Fig. 13 (a) depicts the variation of migration speed. The result implies that the variations are highly synchronized for most conditions. A scatter diagram for V'_{SC} and V_{SP} shown in Fig. 13 (b) confirms a high correlation. Fig. 13 (a) and (b) suggest that cross correlation analysis of the time-stack for the estimation of migration speeds of mega-cusps is trustable.

Figure: 12

Figure: 13

1

2 **5.3** ***Longshore current speeds***

3 Longshore currents are often assumed to be the driving force behind the longshore migration
4 of crescentic bars and rips [Ranasinghe et al., 1999; Ruessink et al., 2000; Van Enckevort and
5 Ruessink 2003]. In absence of current information, Ranasinghe et al. [1999], Ruessink et al.
6 [2000], and Van Enckevort and Ruessink [2003] linked longshore migration to the offshore
7 wave incidence angle θ_0 and to the longshore component of the offshore wave power P_l.
8 Intuitively, P_l is a better proxy for the longshore current than θ_0, as it includes wave height in
9 addition to wave direction. We compared the longshore current speed V_l observed at the Hors
10 pier (y = 115 m) on week days (data per day) to the longshore component of the offshore
11 wave power P_l, which may be used as a proxy for the longshore current. According to Komar
12 [1998], and Van Enckevort and Ruessink [2003], P_l can be expressed as

13

14 $$P_l = \frac{\rho g^2}{32\pi} H_{rms0}^2 T_{1/3} \sin\theta_{1/3} \cos\theta_{1/3} \quad (6)$$

15

16 where ρ is the sea water density (1025 kg/m^3) and g the gravitational acceleration. H_{rms0} is the
17 offshore root-mean-square wave height ($H_{1/3}/\sqrt{2}$). $\theta_{1/3}$ and $T_{1/3}$ are the offshore significant
18 wave angle and wave period respectively. Note that the sign of P_l for waves incident from the
19 north (south) is positive (negative).

The variation of P_l computed from Eq. (6) with the measured wave data are plotted with the observed V_l at the pier in Fig. 14, and the corresponding scatter diagram is shown in Fig.15. The results show that V_l is correlated to the estimated P_l, with $R^2 = 0.48$, and with both P_l and V_l showing local peaks during the 18 energetic events. These results imply the reliability of using the longshore component of wave power as a proxy for the longshore current speeds and compensate V_l which is limited to a data per day.

Figure: 14

Figure: 15

5.4 *Migration speeds of the mega-cusps*

Results of the estimation of longshore migration speeds of the shoreline mega-cusps for two years are shown to demonstrate the unique uses of radar measurements and to discuss the behavior of mega-cusps at the site. In the estimation, as mentioned before, the domain was divided into two parts and the cross correlation analyses were applied to the two domains individually to examine whether there were differences in migration direction and speeds.

In order to minimize the noise associated with the cross-correlation analysis, we found empirically that a 6-hour moving average filter gives smooth results. Fig. 16 shows the variations of longshore migration speeds V_s of the first and second domains filtered with a 6-hour moving average and indicates a strong correlation between them. Fig.17 shows a scatter diagram of the migration speeds estimated in both domains. Although the correlation factor is high R^2 =0.75, the migration speeds in domain 1 are faster by approximately 10%

compared to that of domain 2 and this slight difference may raised due to the data spreading of the higher speeds above 3 m/hr. Hereafter, we average the migration speeds of the domains and compare its variation with the longhsore current V_l and longshore component of the offshore wave power P_l. *Figure: 16* *Figure: 17*

It is intuitively attractive to assume that longshore currents are the driving force behind the migration of longshore coastal features [Ranasinghe et al., 1999; Ruessink et al., 2000; Van Enckevort and Ruessink 2003]. Thus, to illustrate this, we compare in Fig. 18 time series of the average migration speeds V_s of the domains to the measured longshore current speeds V_l at the pier and the longshore component of the wave power P_l as a proxy of longshore current. Fig. 18 reveals that the variations of V_s with V_l and P_l are highly synchronized for most conditions, and it seems that the variations depend mainly on the longshore current speed, which supports the supposition that the longshore migration is forced by the wave-driven longshore current. The consistency is strong with the shoreline mega-cusps migration speeds reaching their local peaks similar to V_l and P_l. The mean and maximum absolute V_s observed in the study are approximately 0.4 m/hr and 4.5 m/hr. These results are of the same order of the crescentic bar migration rates reported by Ruessink et al. [2000] and Van Enckevort and Ruessink [2003]. *Figure: 18*

Fig. 19 (a) and (b) present scatter diagrams of V_s versus V_l and P_l, respectively. Although, there is some scatter, the linear fits are reasonable with a correlation coefficient of

0.53 and 0.47 for V_l and P_l respectively. Ruessink et al. [2000], and Van Enckevort and Ruessink [2003] also found a dependence of crescentic bar migration rates on a similar quantity, the longshore component of wave energy flux. *Figure: 19*

To test whether the majority of the longshore migration speeds vary with the forcing variables $H_{1/3}$ and $\theta_{1/3}$, statistics of the offshore significant wave height $H_{1/3}$ and incidence angle $\theta_{1/3}$ were calculated as shown in Fig. 20. Fig. 20 (a) and (b) shows the frequency of occurrence of offshore wave incidence angles $\theta_{1/3}$ and offshore wave heights $H_{1/3}$ during the two-years study period, while Fig 20 (c) shows the combined frequency occurrence of the two variables. Inspection of Fig. 20 suggests that southern incidence of waves ($\theta_{1/3}< 90°$) occurred more frequently than northern incidence ($\theta_{1/3}> 90°$). The occurrence frequency, the average and the standard deviation of the southern wave incidences are 71%, 66.5°, and 14.2° respectively, while for the northern wave incidences are 27.5%, 100.5°, and 6.5° respectively.

The frequency of occurrence of the migration speeds over the entire two-year study period is shown in Fig. 21 (a). Positive (negative) values are for northern (southern) wave incidence, i.e. the migration is directed southwards (northwards). The diagram shows that shoreline mega-cusps were almost stationary 29% of the time during the total two-year study period when the migration speeds were less than ±0.1 m/hr. Northwards migration occurred 39% of the days, whereas southwards migration occurred on 32%. Also, we observed that migration speeds less than ±0.5 m/hr were observed 54% of the time. The statistical result,

unsurprisingly, shows that the northwards migration rates were typically larger than southwards rates which matches well with the statistical results for the forcing variables and is consistent with the results of the frequency of occurrence for the longshore component of the offshore wave power P_l shown in Fig. 21 (b).

Figure: 20

Figure: 21

The relationship between the migration speeds V_s and the forcing variables $H_{1/3}$ and $\theta_{1/3}$ for the observation period is shown in Fig. 22. V_s have been categorized for classes of every 0.2 m of $H_{1/3}$ between 0.0 to 6.0 m, and every 4° of $\theta_{1/3}$ between 20° to 140°. The mean of V_s within every class is displayed in Fig. 22. The results indicate that as the wave incidence angle deviates from the shore normal, the migration speed increases and vice versa. The maximum migration speed occurred when $\theta_{1/3}$ was between 40° to 45° for northern migration. Ashton al el. [2001] showed that longshore sediment flux is maximum when the relative angle between the wave crests in deep water and the local shoreline orientation is 45°, which implies that migration becomes more active under this condition. On the other hand, for southern migration, the maximum migration speed occurred when $\theta_{1/3}$ was between 100° to 110°. Northern waves seldom have an incidence angle in excess of 120°, so we couldn't compare our results with the discussion of Ashton al el. [2001] for southern migrations.

Figure: 22

6. Concluding Remarks

Intertidal morphology was monitored continuously with an X-band radar at the research pier HORS. The horizontal extent of each radar image was approximately 5.6 km, and hourly-averaged radar images were processed to digitize longshore distributions of shoreline positions. Seasonal variations of longshore mean shoreline positions and their fluctuation intensities observed in the years 2005 and 2006 showed a seasonal change which followed the so-called beach-cycle proposed by Wright and Short [1984]; that is, the mean shoreline position shifted seawards from April to September, and landwards during the following period. The mean shoreline position showed quick recessions and the fluctuation intensities decreased suddenly due to energetic events. During seawards shifts of the mean shoreline position, the intensity of the fluctuation increases. During retreat, it decreases.

The shoreline of Hasaki is consistently characterized by undulating shoreline features "shoreline mega-cusps" that have longshore scales of the order of 10^2-10^3 meters and a temporal scale of days to months. By inspecting the sequence of time-averaged radar images, we observed longshore movement of shoreline mega-cusps within the intertidal region. Therefore, to visualize the temporal and spatial variation of the migration, time-stack images were processed for the two years 2005 and 2006. Longshore pixel intensities close to the waterline were extracted from time-averaged images for every hour. The cross-shore locations of the extractions were shifted in accordance with the observed tide level. Oblique patterns or streaks are observed within the time-stack image, which indicates that shoreline mega-cusps

observed in the intertidal morphologies are migrating in the direction of the streaks and with speeds proportional to the slope of the streaks. Longshore migration speeds of shoreline mega-cusps for the entire study period were estimated by cross correlation analysis of the time-stack image, and their reliability checked. Time series estimates of the average migration speeds V_s were compared to measured longshore current speeds V_l at the pier and the longshore component of the wave power P_l as a proxy for the longshore current, and the results reveal that the variations of V_s with V_l and P_l are highly synchronized for most conditions and that the variations depend mainly on the longshore current speed, which supports the supposition that the longshore migration is forced by the wave-driven longshore current.

Finally, the migration statistics were related to the wave data. Shoreline mega-cusps were observed to be almost stationary 29% of the time period, northwards migration occurred 39%, and southwards migration occurred 32% of the days. The statistical results showed that the northwards migration rates were typically larger than the southwards rates, which agrees well with the statistical results for the forcing variables. The relationship between the migration speeds V_s and the forcing variables $H_{1/3}$ and $\theta_{1/3}$ indicate that the maximum migration speed occurred when $\theta_{1/3}$ was between 40° to 45° for the northern migrations, whereas it was between 100° to 110° for the southern migrations.

The present work illustrates the relationships between migration of shoreline

mega-cusps and the longshore current. Further work is necessary to understand the dynamics of sediment motion within the intertidal zone required to maintain the migration, which is not well understood at the present.

Acknowledgements

The authors are grateful to the members of the Littoral Drift Division, PARI, who provided assistance in radar and wave measurements and results of the depth surveys. Part of this study was financially supported by the Grants-in-Aid of the Japan Society for the Promotion of Science (JSPS).

References

Arzaburu, A.R., Ilic, S., and Gunawardena, Y., [2007] "A study of intertidal bar dynamics using the video system," in *Proc. Coastal sediments '07*, *ASCE*, New Orleans, pp. 1865-1876.

Ashton, A., Murray, A.B., and Arnault, O., [2001] "Formation of coastline features by large-scale instabilities induced by high-angle waves". *Nature*, **414**, pp. 296-300.

Bell, P. S., [1999] "Shallow water bathymetry derived from an analysis of X-band marine radar images of waves," *Coastal Engineering* **37**, pp. 513–527.

Bell, P. S., [2001] "Determination of bathymetry using marine radar images of waves," in

Proc. 4th International Symposium on Ocean Wave Measurement and Analysis, San Francisco, California, Vol. 1, pp. 251–257.

Borge, J.C.N., & Soares, C.G., [2000] "Analysis of directional wave fields using X-band navigation radar," *Coastal Engineering*, **40**, pp. 375-391.

Bruner, K.R., & Smosna, R.A., [1989] "The movement and stabliziation of beach sand on transverse bars, Assateague Island, Virginia," *Journal of Coastal Research*, **5 (3)**, pp. 593-601.

Bruun, P., [1954] "Migrating sand waves or sand humps, with special reference to investigations carried out on the Danish north coast sea," in *Proc. 5th Coastal Engineering Conf. AXE,* New York, pp. 269-295.

Calvete, D., Dodd, N., Falques, A., and Van Leeuwen, S.M., [2005] "Morophological development of rip channel system: Normal and near-normal wave incidence," *Journal of Geophysical Research*, **110**, C10006, doi: 10.1029/2004JC002803.

Dalon, M.M., Haller, M., and Allan, J., [2007] "Morphological characteristics of rip current embayments," in *Proc. Coastal sediments '07*, *ASCE*, New Orleans, pp. 2137-2150.

Davidson-Arnott, R.G., & Van Heyningen, A.G., [2003] "Migration and sedimentology of longshore sandwaves, Long Point, Lake Erie, Canada," *Journal of Sedimentology*, **50**, pp.1123–1137.

De Melo Apoluceno, D., Howa, H., Dupuis, H., and Oggian, G., [2002] "Morophodynamics of

ridge and runnel system during summer," *Journal of Coastal research,* **SI 36**, pp. 222-230.

Dolan, R., [1971] "Coastal landforms: crescentic and rhythmic," *Geological Society of America Bulletin*, **82**, pp. 177-180.

Esteves, L. S., Williams, J. J., and Bell, P. S., [2007] "Assessing nearshore bar movements during storms using time-averaged X-band radar images," in *Proc. Coastal sediments '07, ASCE*, New Orleans, pp. 1886-1899.

Guillèn, J., Stive, M.J.F., and Capoblianco, M., [1999] "Shoreline evolution of the Holland coast on decadal scale," *Journal of Earth Surface Processes and Landforms*, **24**, pp. 517-536.

Hasan, G.M.J., & Takewaka, S., [2007]" Observation of a stormy wave field with X-band radar and its linear aspects," *Coastal Engineering Journal*, *JSCE* **49(2)**, p.p. 149–171.

Holman, R.A., Symonds, G., Thornton, E.B., and Ranasinghe, R., [2006] "Rip spacing and persistence on an embayed beach," *Journal of Geophysical Research* **111**, C01006, doi:10.1029/2005/JC002965.

Jesse E. McNinch, [2007] "Bar and swash imaging radar (BASIR): A mobile X-band radar designed for mapping nearshore sand bars and swash-defined shorelines over large distances," *Journal of Coastal Research* **23(1),** pp. 59-74.

Katoh, K., and Yanagishima, S., [1995] “Changes of sand grain distribution in the surf zone,” in *Proc. Coastal Dynamics ’99, Am. Soc. Of Eng., NewYork*, pp. 335-364.

Komar, P.D., [1971] “Nearshore cell circulation and the formation of giant cusps," *Geological Society of America Bulletin*, **82**, pp. 177-180.

Komar, P.D., [1998] “Beach processes and sedimentation,” *Prentice Hall, Inglewood Cliffs*, New Jersey, pp. 429.

Konicki, K.M., & Holman, R.A., [2000] “The statistics and kinematics of transverse sand bars on an open coast,” *Marine Geology*, **169**, pp. 69-101.

Kuriyama, Y., & Lee, J.H., [2001] “Medium-term beach profile change on a bar-trough region at Hasaki, Japan, investigated with complex principal component analysis,” in *Proc. Coastal Dynamics '01*, *ASCE*, pp. 959-968.

Lofon, V., De Melo Apoluceno, D., Dupuis, H., Michel, D., Howa, H., and Froidefond, J.M., [2004] “Morphdynamics of nearshore rhythmic sandbars in a mixed-energy environment (SW France): I. Mapping beach changes using visible satellite imagery,” *Journal of Estuarine, Coastal and Shelf Science*, **61**, pp. 289-299.

Lofon, V., Dupuis, H., Butel, R., Castelle, B., Michel, D., Howa, H., and De Melo Apoluceno, D., [2005] “Morphdynamics of nearshore rhythmic sandbars in a mixed-energy environment (SW France): 2. Physical forcing analysis,” *Journal of Estuarine, Coastal and Shelf Science*, **65**, pp. 449-462.

Ranasinghe, R., Symonds, G., Black, K., and Holman, R., [2000] "Processes governing rip spacing, persistence and strength in a swell dominated, microtidal environment," in *Proc. of the International Conference on Coastal Engineering (ICCE), Sydney, Australia, ASCE*, pp. 455–467.

Ranasinghe, R., Symonds, G., and Holman, R., [1999] "Quantitative characterisation of rip dynamics via video imaging," in *Proc. Coastal Sediments'99, New York: ASCE*, pp. 987– 1002.

Ruessink, B.G., & Jeuken, M.C.J., [2002] "Dunefoot dynamics along the Dutch coast," *Journal of Earth Surface Processes and Landforms*, **27**, pp.1043– 1056.

Ruessink, B.G., Bell, P.S., Van Enckevort, I.M.J. and Aarninkhof, S.G.J., [2002] "Nearshore bar crest location quantified from time-averaged X-band radar images," *Coastal Engineering*, **45**, pp. 19-32.

Ruessink, B.G., Van Enckevort, I.M.J., Kingston, K.S., and Davidson, M.A., [2000] "Analysis of observed two- and three-dimensional nearshore bar behaviour," *Marine Geology*, **169**, pp. 161–183.

Sallenger, A. H., [1979] "Beach cusp formation," *Marine Geology*, **29**, pp. 23–37.

Sallenger, A.H., Holman, R.A., and Birkemerier, W., [1985] "Storm-induced response of a nearshore-bar system," *Marine Geology*, **64**, pp. 237-257.

Shepard, F.P., [1952] "Revised nomenclature for depositional coastal features," *Amr. Assoc.*

Petroleum Geologists Bull., **36(10)**, pp. 1902-1912.

Short, A.D., Hesp, P.A., [1982] "Wave, beach and dune interactions in South Eastern Australia," *Marine Geology*, **48**, pp. 259-284.

Stewart, C.J., & Davidson-Arnott, R.G.D., [1988] "Morphology, formation and migration of longshore sandwaves; Long Point, Lake Erie Canada," *Marine Geology*, **81**, pp. 63–77.

Takewaka, S. & Nishimura, H., [2005] "Wave run-up analyses during a storm event with nautical X-band radar," in *Proc. Asian and Pacific Coasts on CD-Rom (APAC 2005)*, Korea.

Takewaka, S. [2005] "Measurements of shoreline positions and intertidal foreshore slopes with Xband marine radar system," C*oastal Engineering Journal, JSCE,* **47**, pp. 91–107.

Thevenot, M.M., & Kraus, N.C., [1995] "Longshore sand waves at Southampton Beach, New York: observation and numerical simulation of their movement," *Marine Geology*, **126**, pp. 249-269.

Thornton, E.B., MacMahan, J., and Sallenger J.A.H., [2007] "Rip currents, mea-cusps, and eroding dunes," *Marine Geology*, **240**, pp. 151-167.

Turner, I. L., Whyte, D., Ruessink, B.G. and Ranasinghe, R., [2007] "Observations of rip spacing, persistence and mobility at a long, straight coastline," *Marine Geology*, **236**, pp. 209-221.

1 Van Enckevort, I.M.J., Ruessink, B.G., Coco, G., Suzuki, K., Turner, I.L., Plant, N.G. and
2 Holman, R.A., [2004] "Observations of nearshore crescentic sandbars," *Journal of*
3 *Geophysical Research*, **109**, C06028, doi:10.1029/2003JC002214.
4 Van Enckevort, I.M.J., and Ruessink, B.G., [2003] "Video observations of nearshore bar
5 behavior. Part 2: longshore non-uniform variability," *Journal of Continental Shelf*
6 *Research*, **23**, pp. 513-532.
7 Van Houwelingen, S., Masselink, g., and Bullard, J., [2006] "Characteristics and dynamics of
8 multiple intertidal bars, north Lincolnshire, England," *Journal of Earth Surface*
9 *Processes and Landforms*, **31**, doi: 10.1002/esp.1276, pp. 428-443.
10 Verhagen, H.J., [1989] "Sand waves along the Dutch coast," *Coastal Engineering Journal*, **13**,
11 pp.129–147.
12 Wright, L.D. & Short, A.D., [1984] "Morphodynamic variability of surf zones and beaches,"
13 *Marine Geology*, **56**, pp. 93-118.
14 Wright, L.D., [1980] "Beach cut in relation to surf zone morphdynamics," in *Proc. of 17th*
15 *International Conf. on Coastal Engineering, ASCE*, pp. 978-996.
16 Young, I.R., Rosenthal, W. and Ziemer, F., [1985] "A three-dimensional analysis of marine
17 radar images for the determination of ocean wave directionality and surface
18 currents," *Journal of Geophysical Research*, **90(C1)**, pp. 1049–1059.

19 Table 1: Observations of longshore migrations of coastal features

Table 2: Energetic events within the study period 2005 and 2006.

Coastal feature	Site	Data Set	Methodology	Length (m)	Migration rate	Reference
Crescentic Bar	Duck, NC, USA	(4-times) in 2 weeks	Periodical survey	≈ 300	20 m/day	Sallenger *et al.* [1985]
	Egmond, NL	(30-times) in 6 weeks	Video observation	575	0-150 m/day	Ruessink *et al.* [2000]
	Noordwijk, NL	(Daily) 3.4 years	Video observation	710-1360	0-180 m/day	Van Enckevort & Ruessink [2003]
	Duck, NC, USA	(Hourly) 8 weeks	Video observation	173-855	0-60 m/day	Van Enckevort *et al.* [2004]
	Miyazaki, Kyushu, JP	(Hourly) 10 weeks	Video observation	200-966	0-50 m/day	Van Enckevort *et al.* [2004]
	Queensland, AU	(Hourly) 13 weeks	Video observation	151-1528	0-45 m/day (inner bar)	Van Enckevort *et al.* [2004]
				224-1608	0-35 m/day (outer bar)	
	Noordwijk, NL	(Hourly) 43 weeks	Video observation	441-1503	0-60 m/day (inner bar)	Van Enckevort *et al.* [2004]
				828-2120	0-25 m/day (outer bar)	
	Gironde, FR	(16-times) in 15 years	Spot satellite images	≈ 740	1 m/day	Lafon *et al.* [2004, 2005]
Transverse Bars	Duck, NC, USA	(Daily) 10 years	Video observation	79-172	40 m/day	Konicki & Holman [2000]
Rips	Palm beach, AU	(Daily)1.6 years	Video observation	≈ 100	0-20 m/day	Ranasinghe *et al.* [2000]
	Palm beach, AU	(Daily) 4 years	Video observation	≈ 178	0-20m/day	Holman *et al.* [2006]
	Queensland, AU	(Daily) 3 years	Video observation	≈ 209	0-50m/day	Turner *et al.* [2007]
Ridge and Runnel	Gironde, FR	(16-times) in 3 years	Shoreline maps + P. survey	≈ 480	1.7 m/day	De Melo Apoluceno *et al.* [2002]
	Gironde, FR	(16-times) in 15 years	Spot satellite images	≈ 420	2.4-3.1 m/day	Lafon *et al.* [2004, 2005]
	North Lincolnshire, UK.	(1 per year) in 9 years	Arial photos + Lidar images	-	1 m/day	Van Houwelingen *et al.* [2006]
	Ceveleys, UK	(Hourly) 3 weeks	Video observation+ P. survey	-	-	Arzaburu *et al.* [2007]
Shoreline mega-cusps	Monterey, CA, USA	(6-times) in 70 days	Periodic survey	≈ 200	3.4 m/day	Thornton *et al.* [2007]
Shoreline sandwaves	Lake Erie, CA	-	Video observation	500-2500	150-300 m/year	Stewart & Davidson-Arnott [1988]
	Dutch coast, NL	(1 per year) in 100 years	Arial photos + P. survey	5500	65 m/year	Verhagen [1989]
	Southampton, NY, USA	(5-times) in 16 month	Periodic survey	750	350 m/year	Thevenot & Kraus [1995]
	Hollandcoast, NL	(1 per ear) in 25 years	Arial photos	2000-3000	150-200 m/year	Guillèn *et al.* [1999]
	Dutch coast, NL	(1 per year) in 150 years	Periodic survey	3500-10000	0-200 m/year	Ruessink & Jeuken [2002]
	Lake Erie, CA	(2~3 per ear) in 7 years	Periodic survey	350-1500	100-300 m/year	Davidson-Arnott &Heyningen [2003]
			Arial photos + P. survey			

Event No.	Date of event peak (h/d/m/y)	Days from 2005/01/01	Peak wave height $H_{1/3}$ (m)	Period at peak wave height $T_{1/3}$ (sec)	Angle at peak wave height $\theta_{1/3}$ (degree)	Event duration (hours)
1	12:00/17/01/2005	16.5	6.14	13.5	108	72
2	04:00/20/02/2005	50.2	3.52	10.4	83	20
3	12:00/04/03/2005	62.5	3.90	7.8	85	16
4	22:00/13/05/2005	132.9	3.67	9.9	81	22
5	22:00/26/07/2005	206.9	3.69	12.1	33	18
6	16:00/25/09/2005	267.6	5.43	9.6	100	52
7	12:00/06/12/2005	339.5	3.78	11.7	106	32
8	04:00/23/12/2005	356.1	3.51	11.8	106	10
9	00:00/15/01/2006	379.0	4.11	8.0	109	20
10	04:00/16/04/2006	470.1	3.83	9.4	78	36
11	08:00/28/05/2006	512.3	3.64	8.9	39	8
12	08:00/05/09/2006	612.3	4.66	15.2	54	58
13	20:00/26/09/2006	633.8	4.08	8.9	70	10
14	16:00/07/10/2006	644.6	5.48	12.7	109	54
15	08:00/16/10/2006	653.3	3.76	9.9	69	20
16	04:00/25/10/2006	662.1	6.47	11.9	100	72
17	00:00/21/11/2006	689.0	4.37	11.9	74	44
18	04:00/27/12/2006	725.1	5.13	11.3	44	24

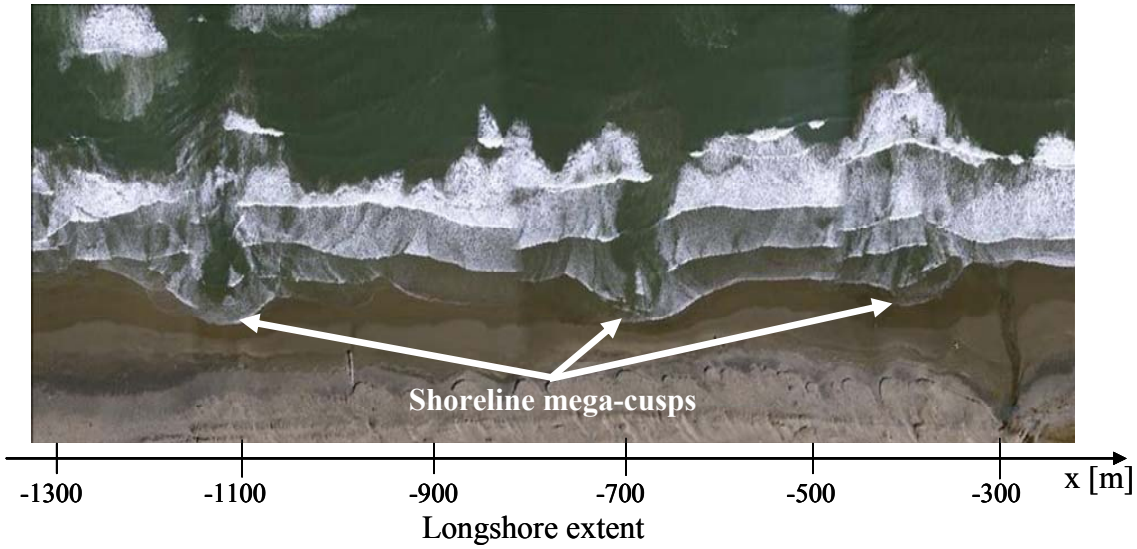

Figure 1: Aerial photograph (12hr 08/November/2006) of Hasaki coast exhibiting the shoreline mega-cusps.

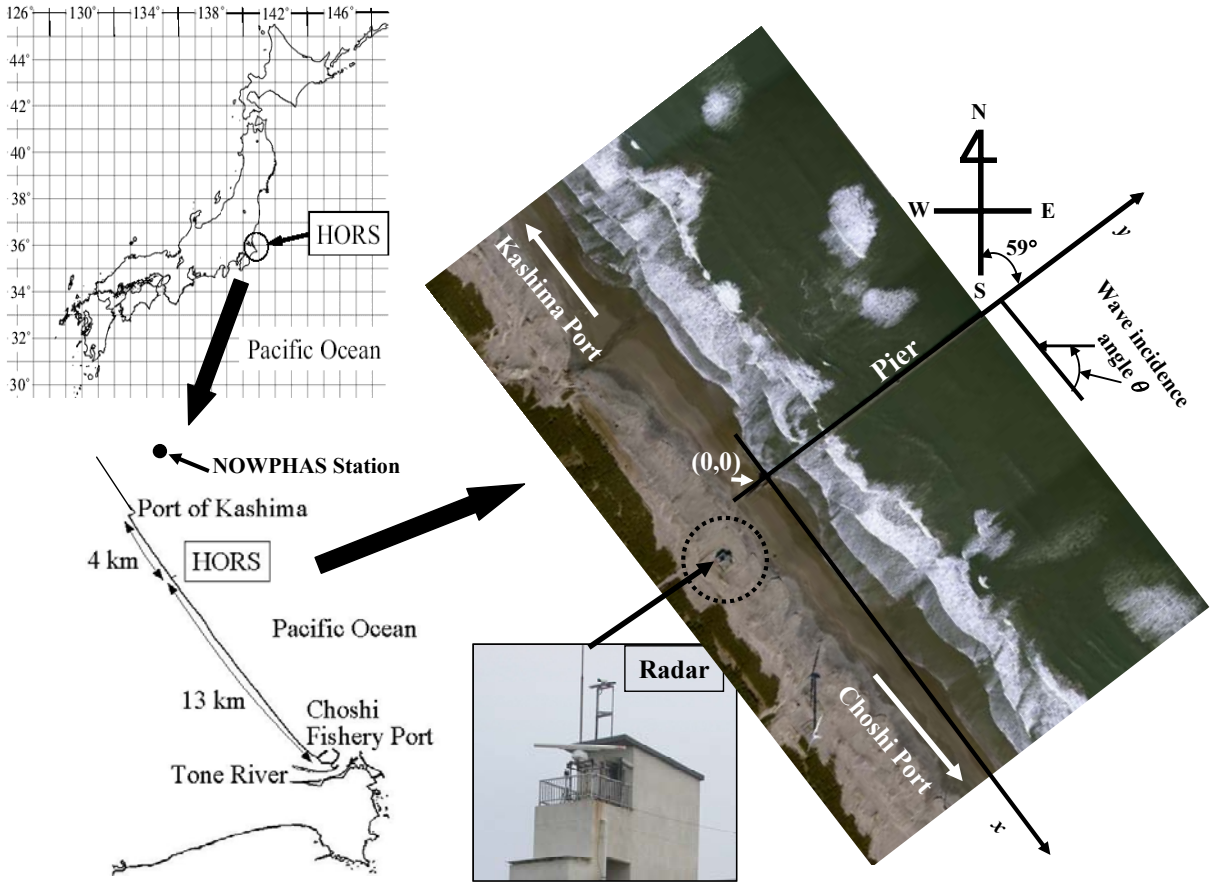

Figure 2: Research Pier HORS

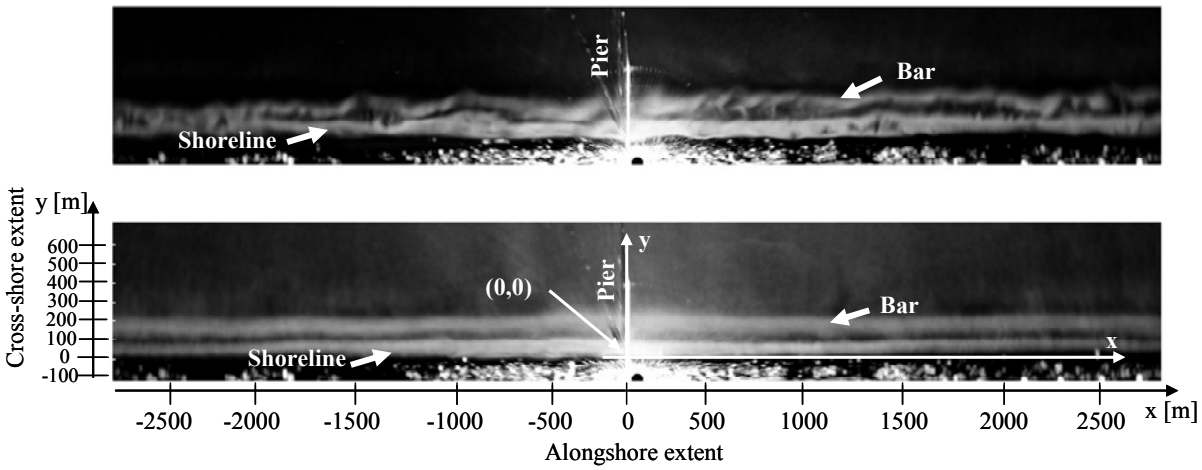

Figure 3: Time averaged echo images and coordinate system. Upper panel: calm conditions (18hr 20/April/2006). Lower panel: stormy conditions (23hr 15/September/2005).

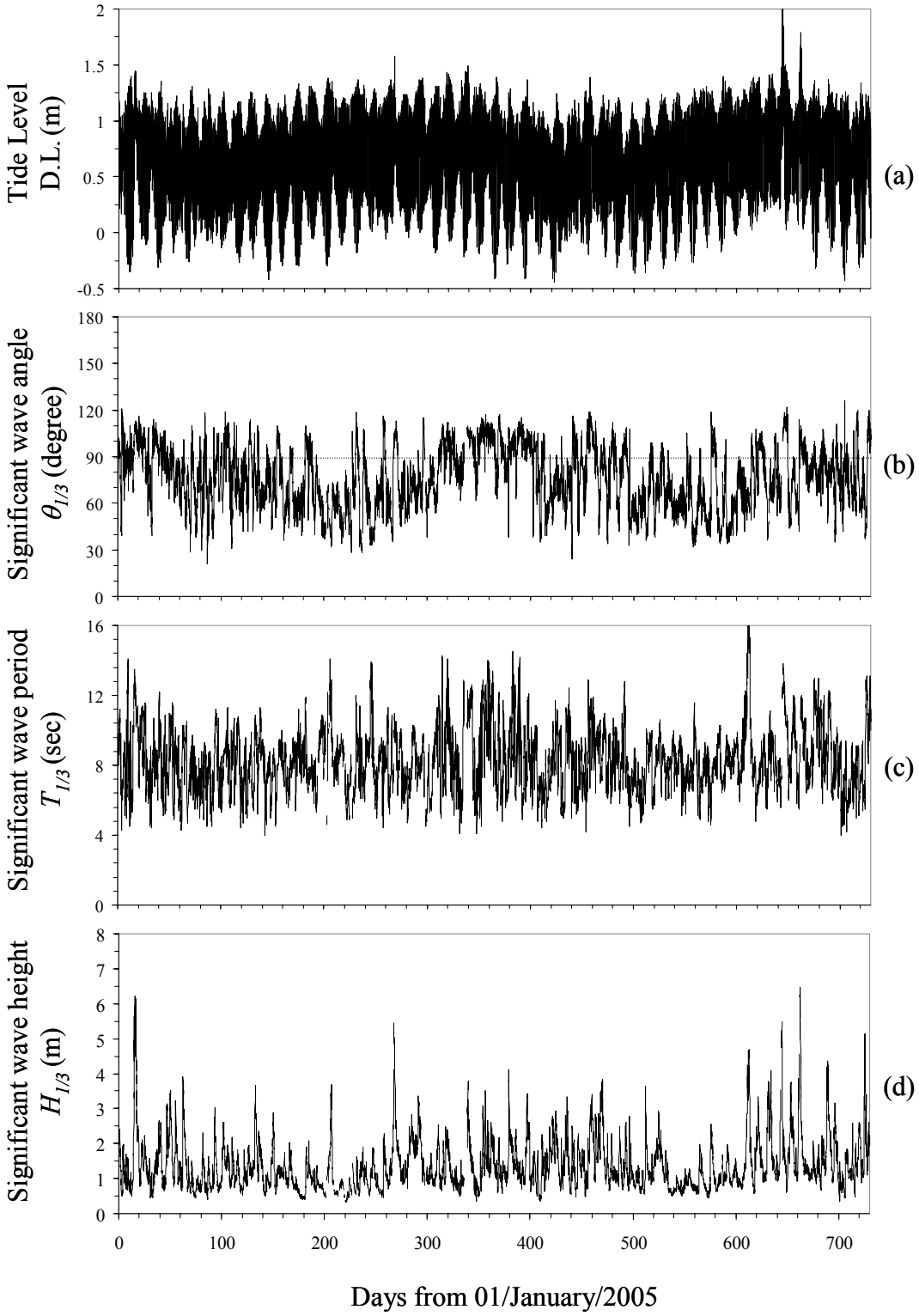

Figure 4: Time histories of (a) tide level, (b) $\theta_{1/3}$, (c) $T_{1/3}$, and (d) $H_{1/3}$. Tide level measured at Choshi Fishery Port, and wave data $\theta_{1/3}$, $T_{1/3}$, and $H_{1/3}$ measured at Kashima Port.

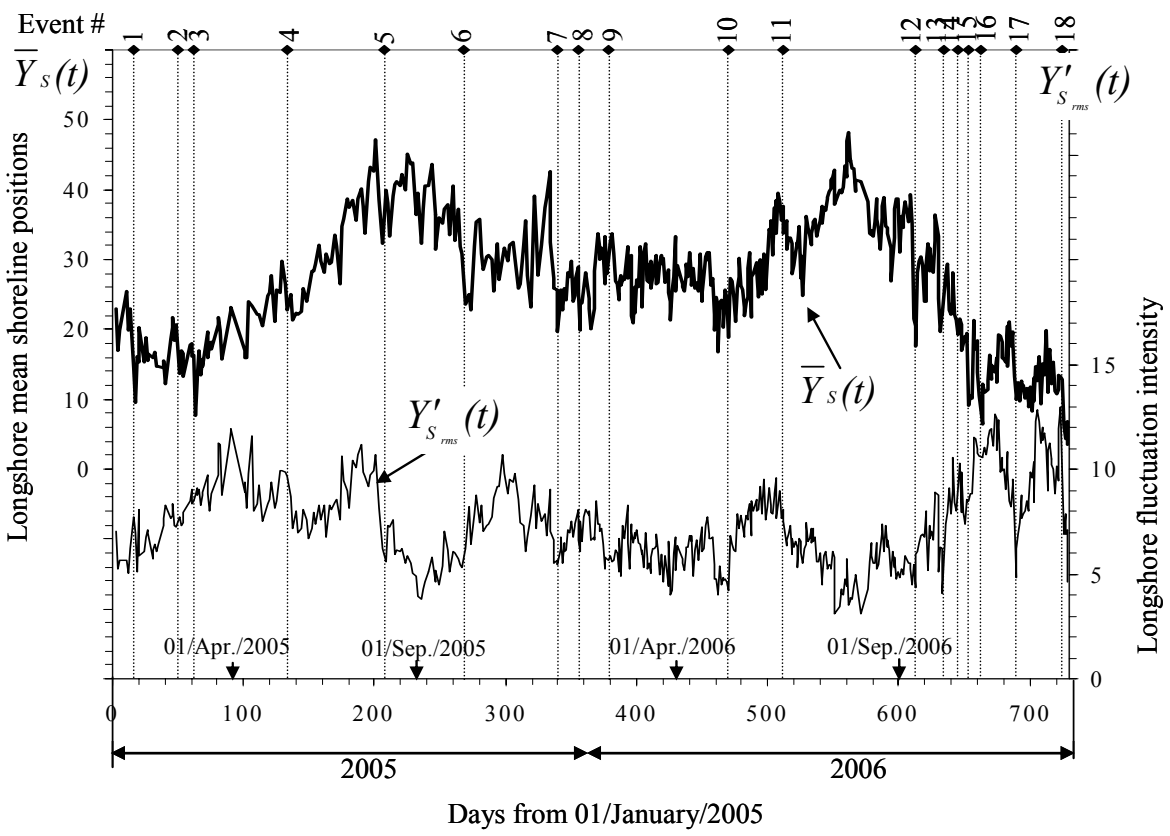

Figure 5: Variations of longshore mean shoreline locations and longshore fluctuation intensity. Numbers listed on the upper horizontal indicate energetic events listed in Table 1.

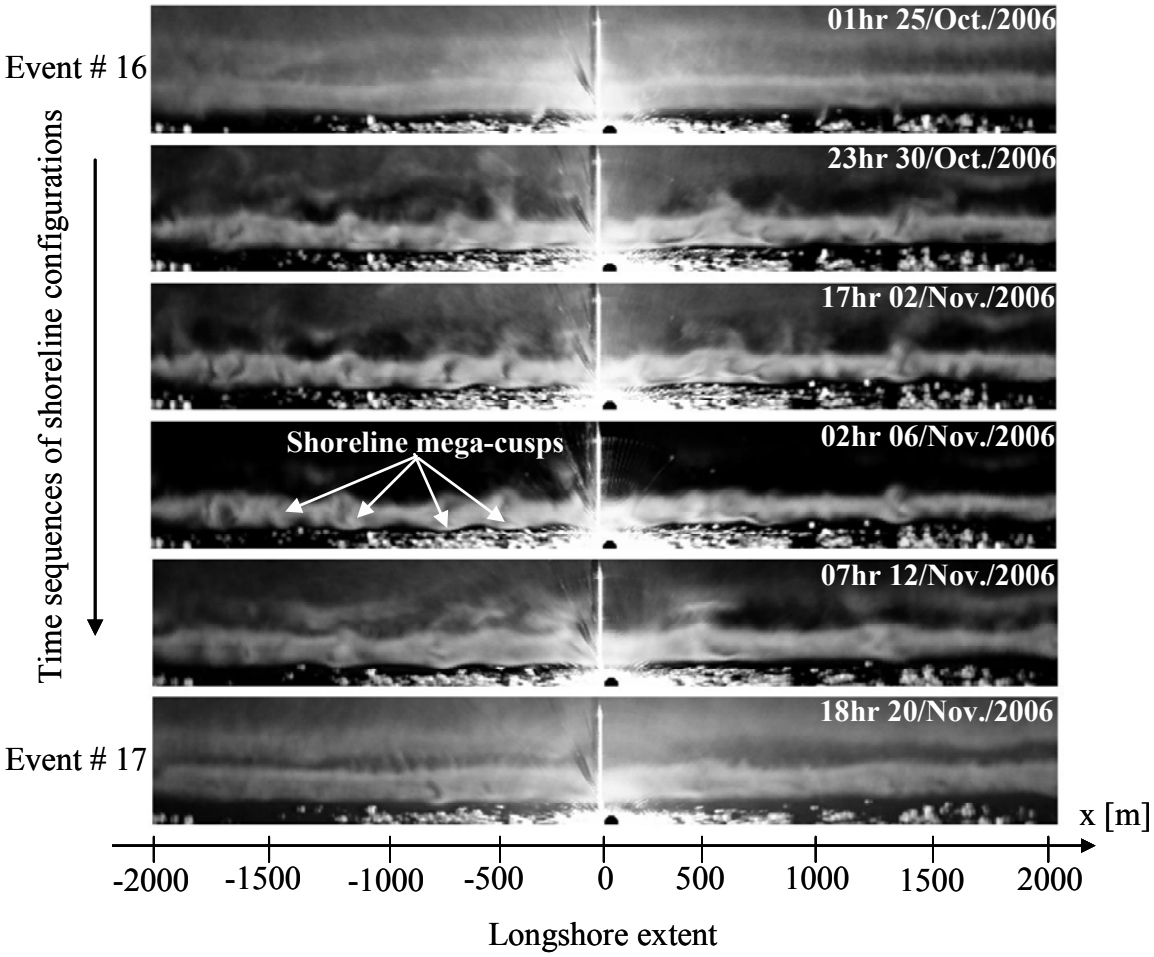

Figure 6: Time-averaged radar images showing time sequences of shoreline configurations occurring between the two energetic events number 16 and 17.

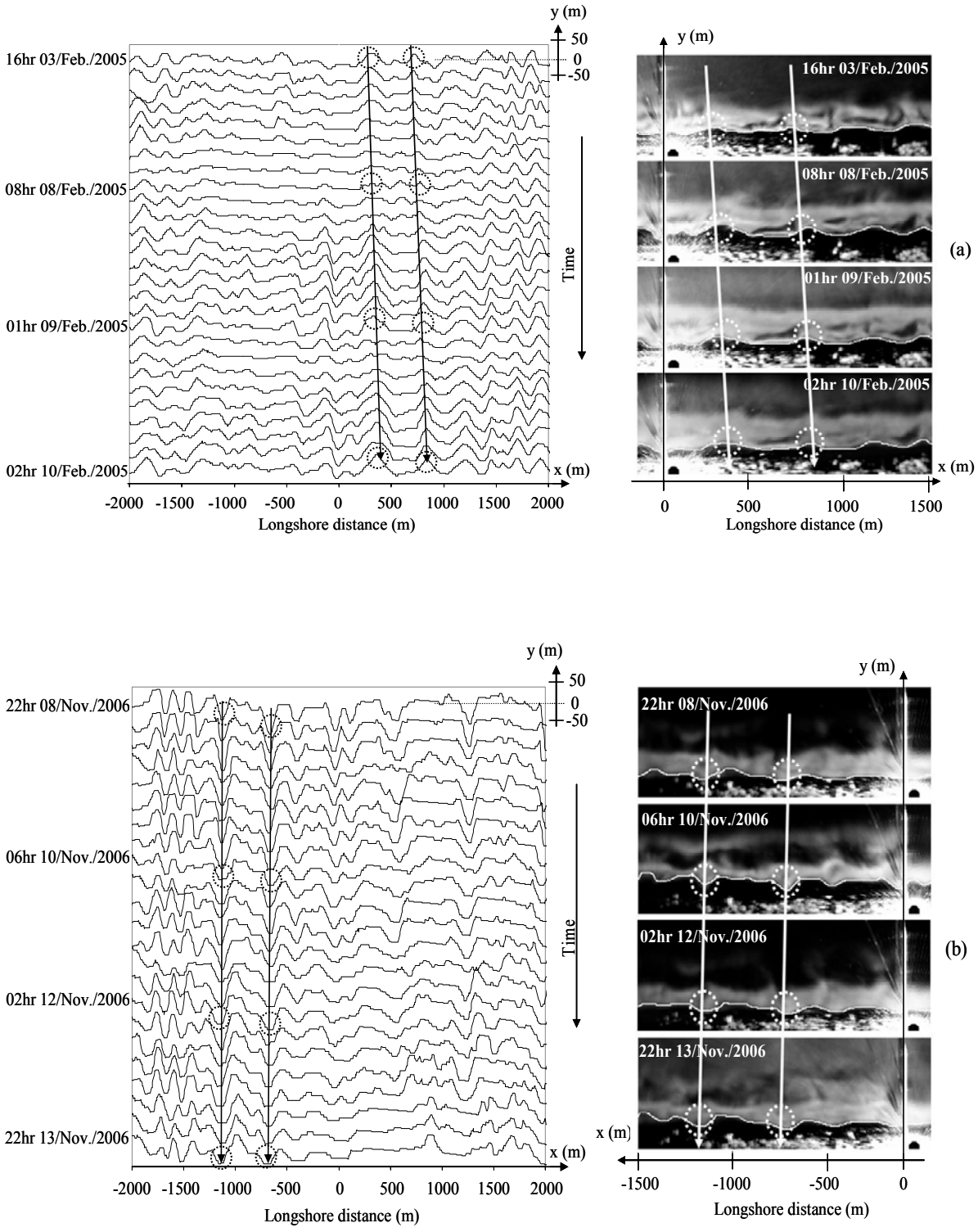

Figure 7: Examples of time histories of longshore distributions of digitized shoreline positions. (a) Migration of mega-cusps towards positive direction, and (b) Migration of mega-cusps towards negative direction. Dashed circles indicate mega-cusp's horns in (a) and embayments in (b).

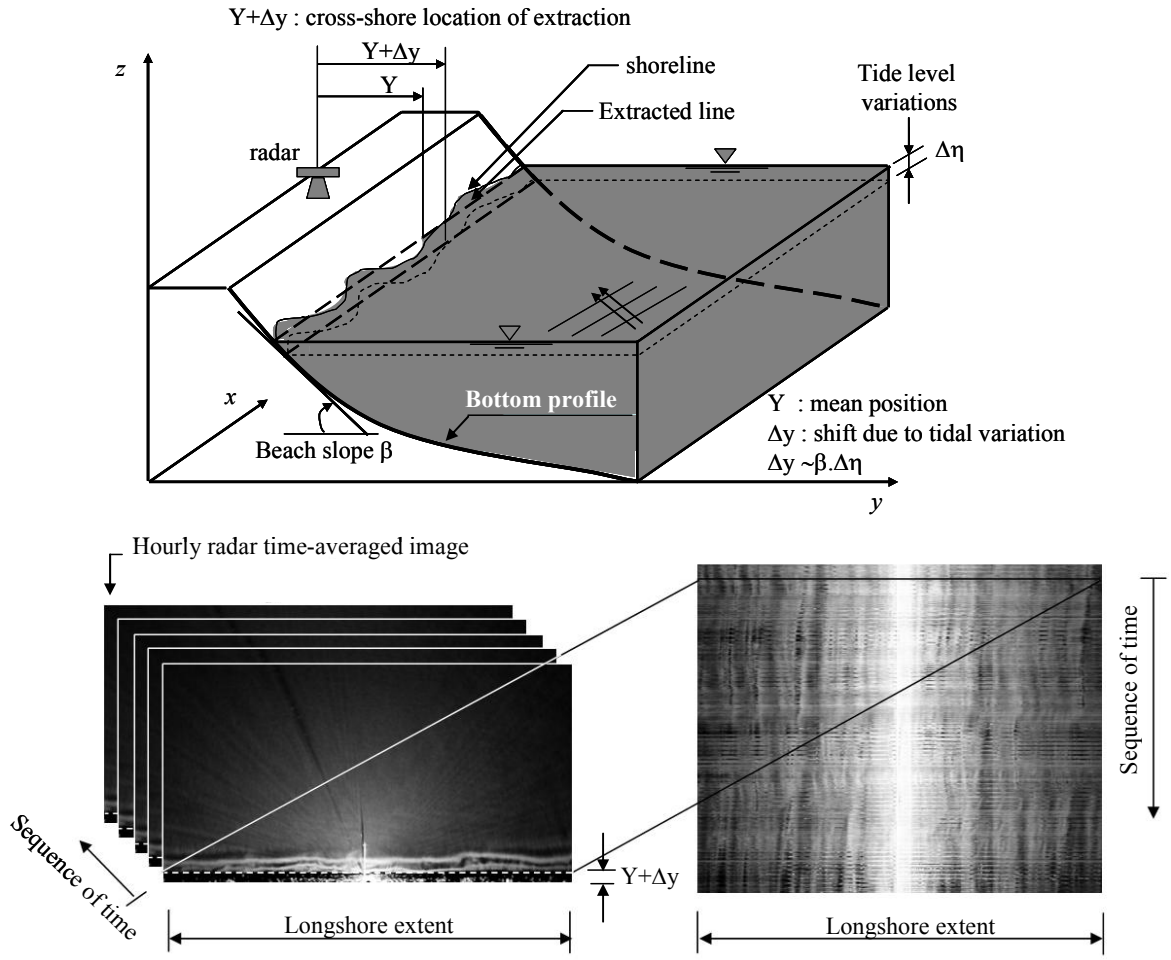

Figure 8: Processing of longshore time-stack from series of time-averaged echo signals.

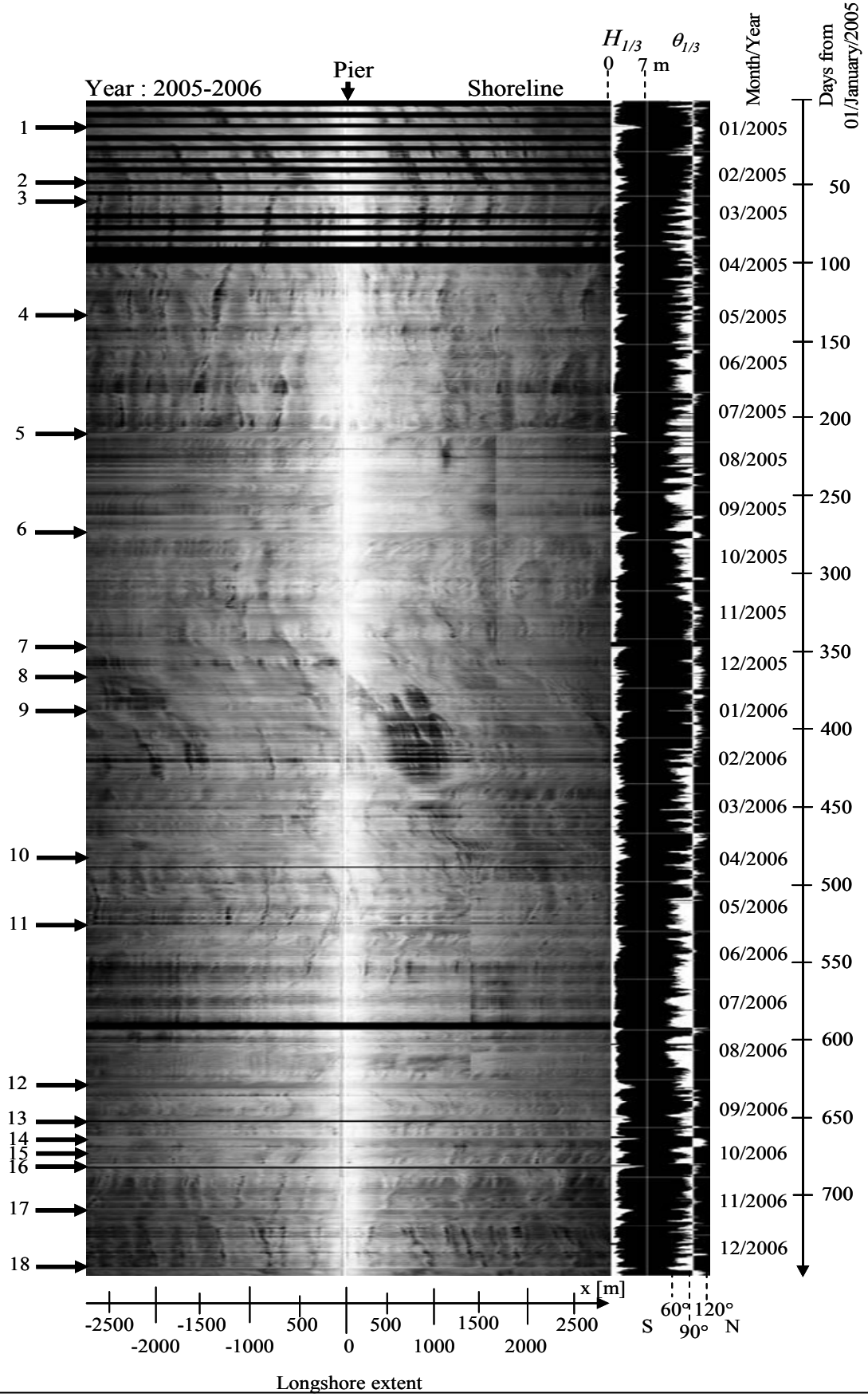

Figure 9: Time-stack of longshore migrations of shoreline mega-cusp locations observed in 2005-2006. $H_{1/3}$: significant wave height, full scale = 7 m. $\theta_{1/3}$: Significant wave angle, S = southern incidence, N = northern incidence. Number and arrows at the left side represent energetic events listed in Table 1.

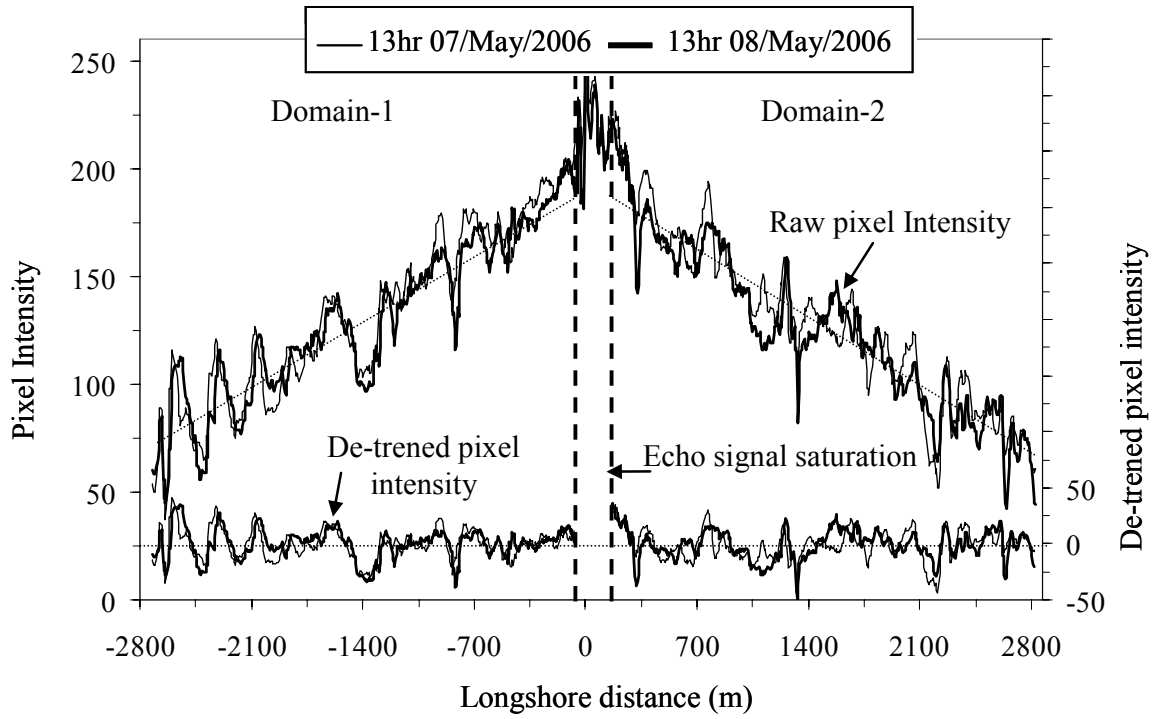

Figure 10: Domain1 and 2 for the cross correlation analyses. Raw and de-trended pixel intensities are shown.

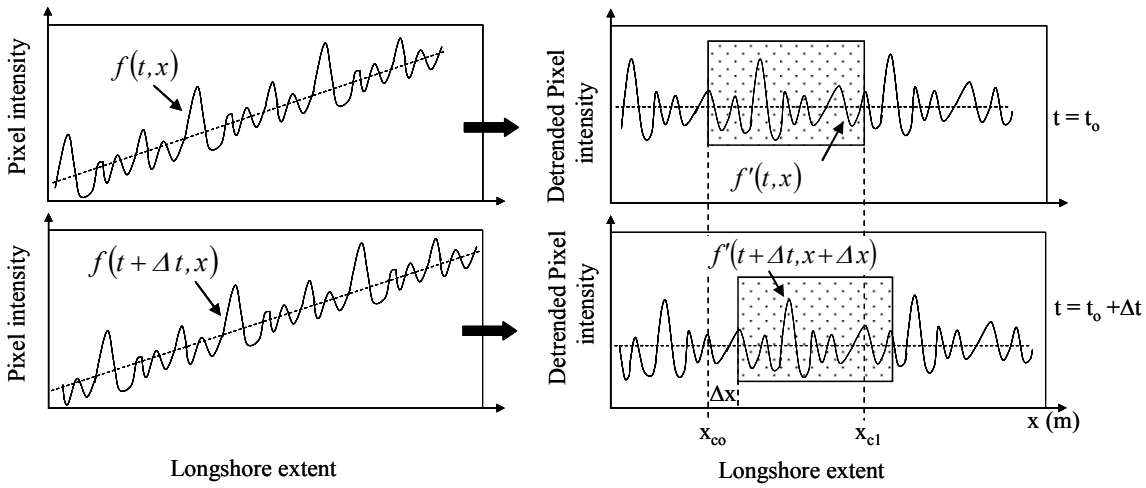

Figure 11: Schematic diagram showing the definition of different variables used in the cross-correlation analysis method.

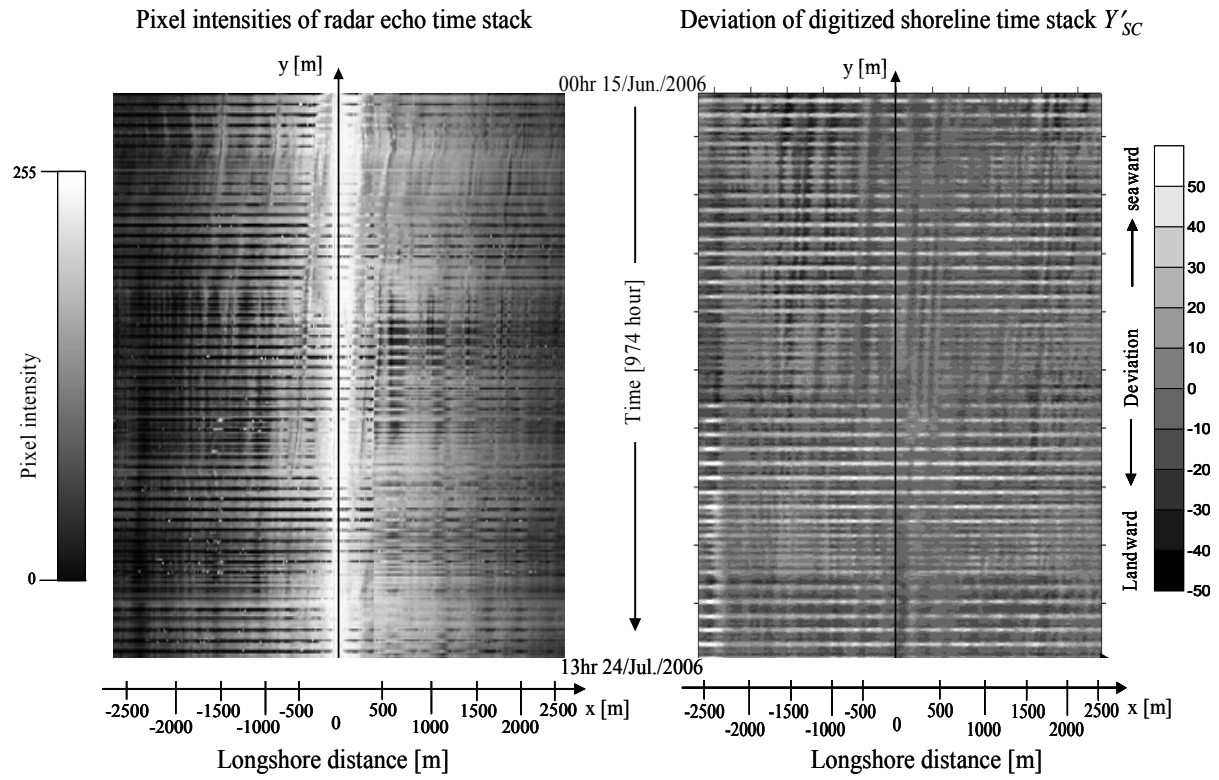

Figure 12: Comparison of time-stack of the deviation of digitized shoreline $Y'_{SC}(t, x)$ (right panel), and pixel intensities time-stack of radar echo (left panel) for the period of 00hr 15/June/2006 – 13hr 24/July/2006.

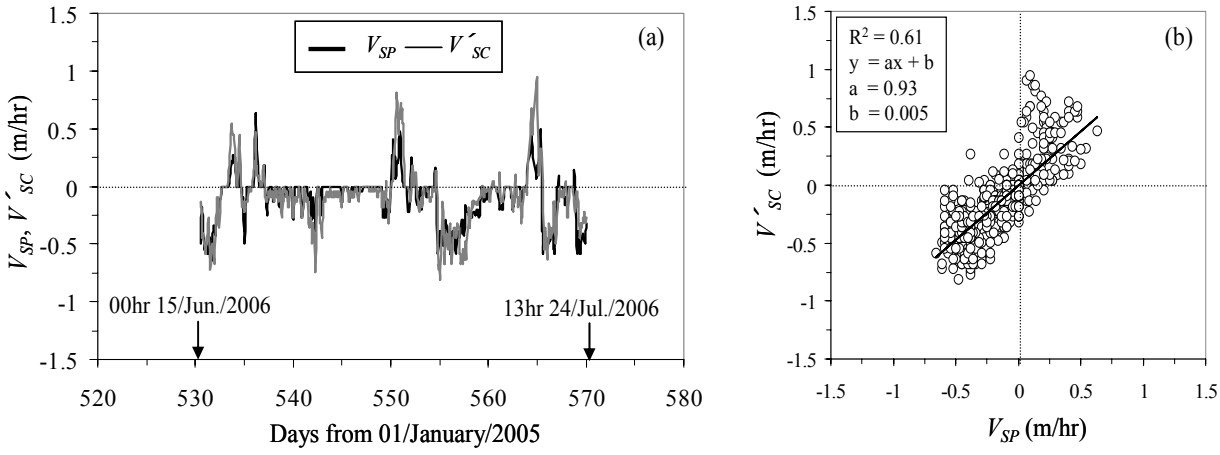

Figure 13: (a) Variations of migration speed V_{SP} estimated from pixel intensity time-stack. V'_{SC} estimated from the deviation lines $Y'_{SC}(t, x)$. (b) Comparison between V_{SP} and V'_{SC} for the period of 00hr 15/June/2006 – 13hr 24/July/2006.

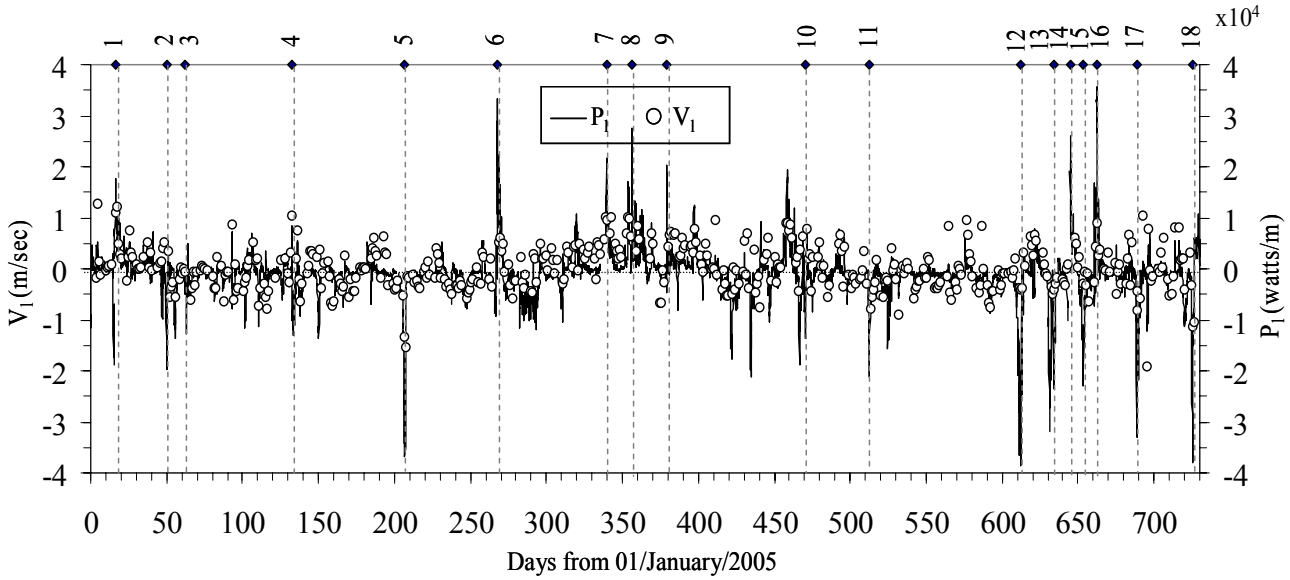

Figure 14: Variations of longshore current velocity V_l observed at the pier and the longshore component of the offshore wave power P_l. Numbers listed on the upper horizontal indicate energetic events listed in Table 1.

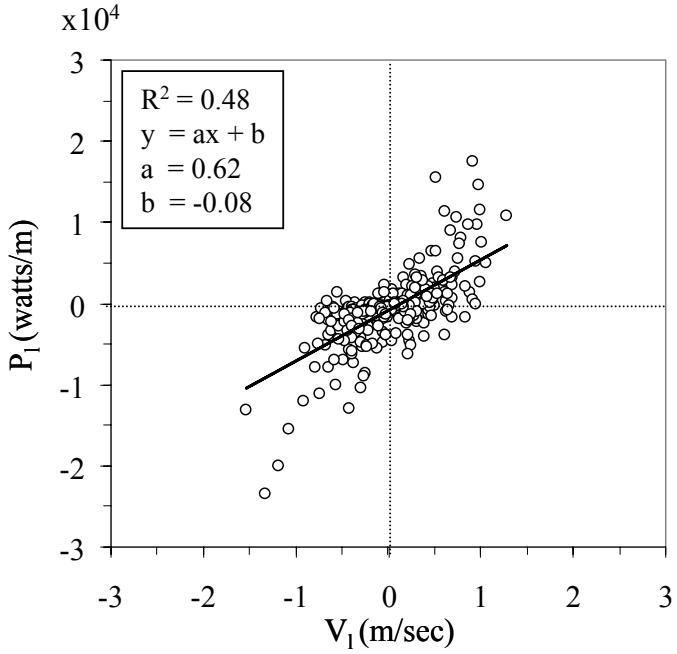

Figure 15: Comparison between longshore current velocities V_l observed at the pier and the longshore component of the offshore wave power P_l

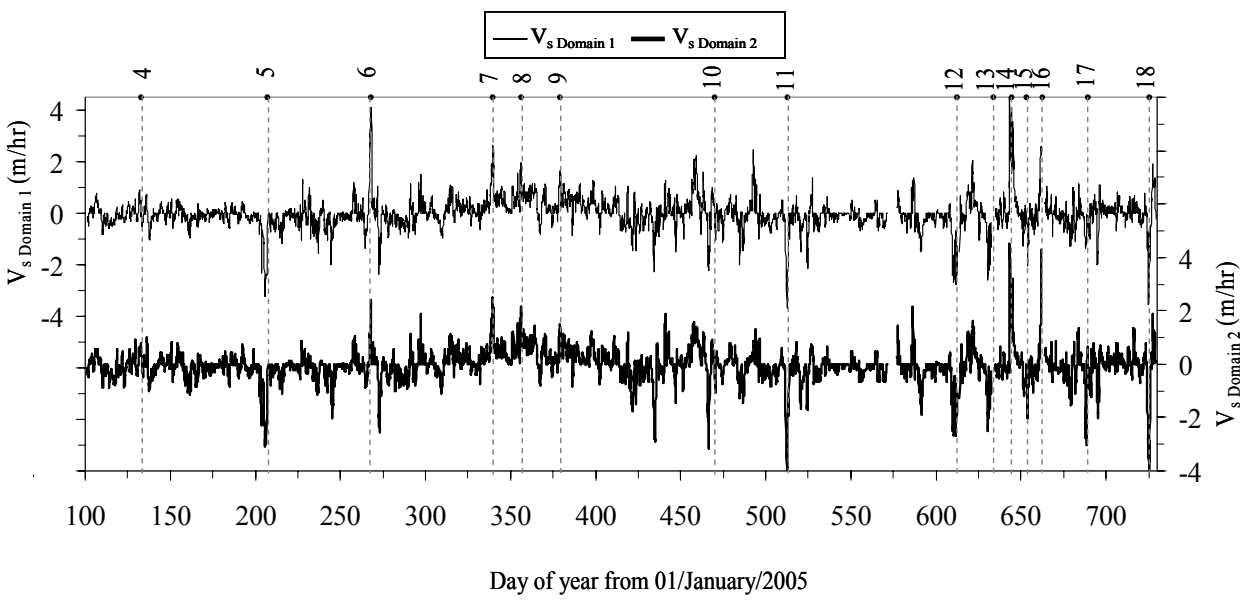

Figure 16: Varations of migration speeds estimated from cross corrleation analyses in domain 1 and 2. Numbers listed on the upper horizontal indicate energetic events listed in Table 1.

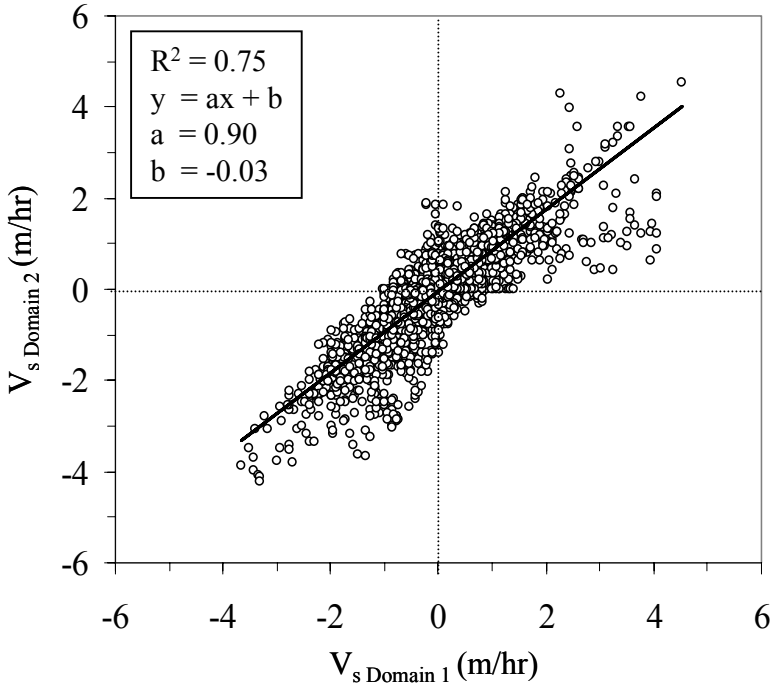

Figure 17: Comparison of migration speeds of domain1 and 2.

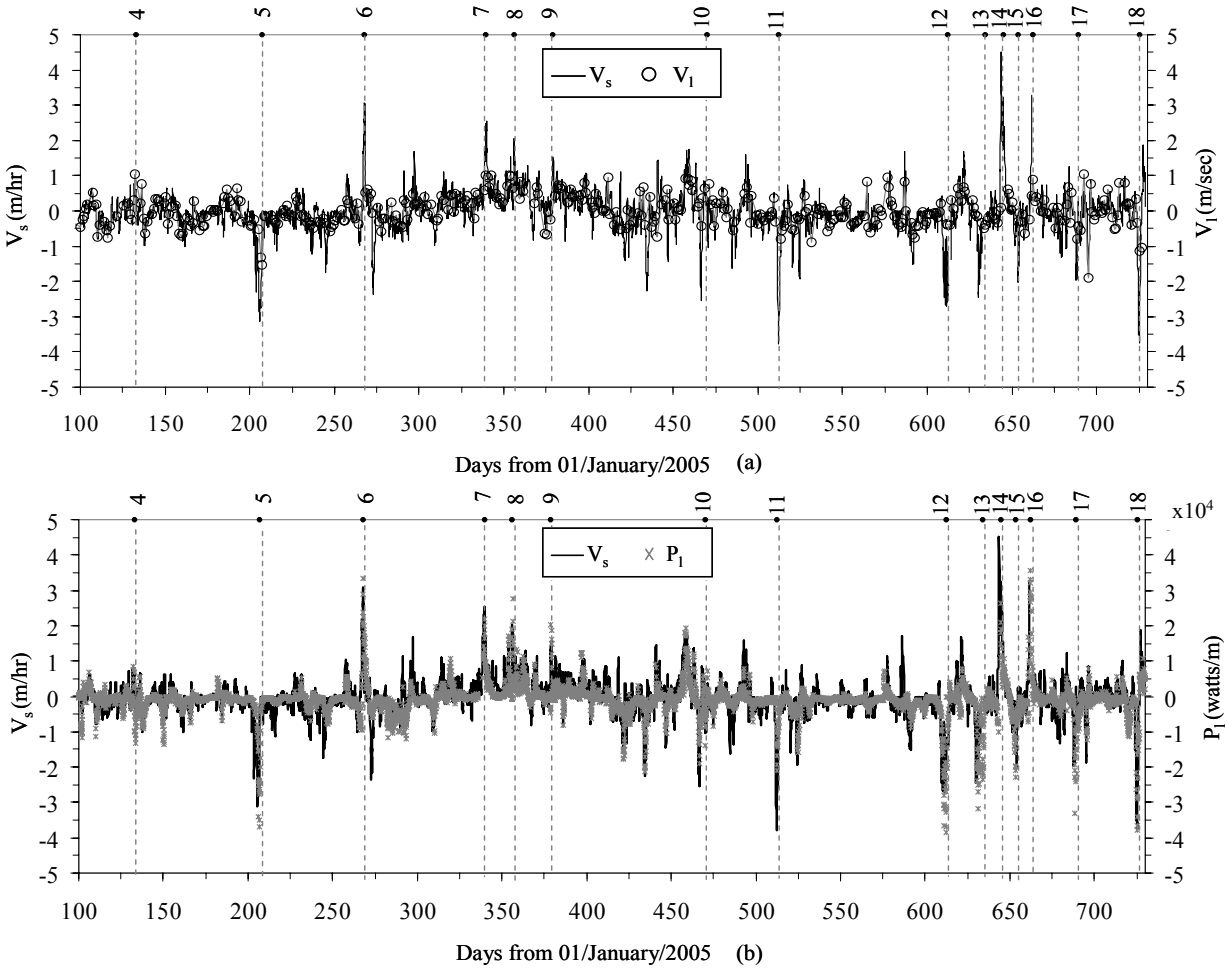

Figure 18: (a) Variations of averaged V_s and V_l; (b) Variations of averaged V_s and P_l. Numbers listed on the upper horizontal indicate energetic events listed in Table 1.

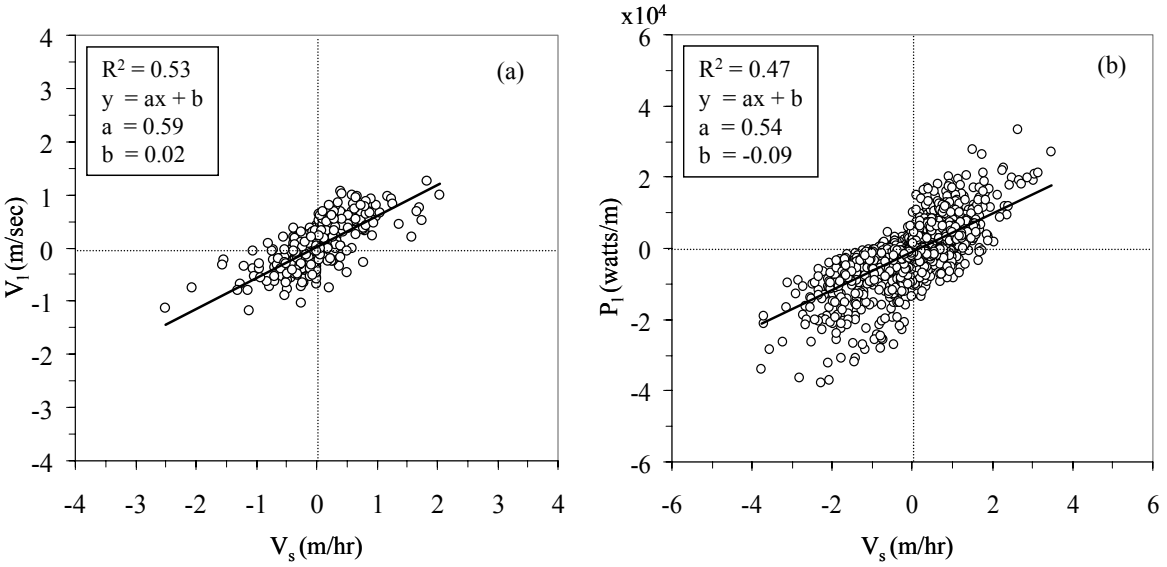

Figure 19: (a) Comparison between averaged V_s and V_l, and (b) Comparison between averaged V_s and P_l.

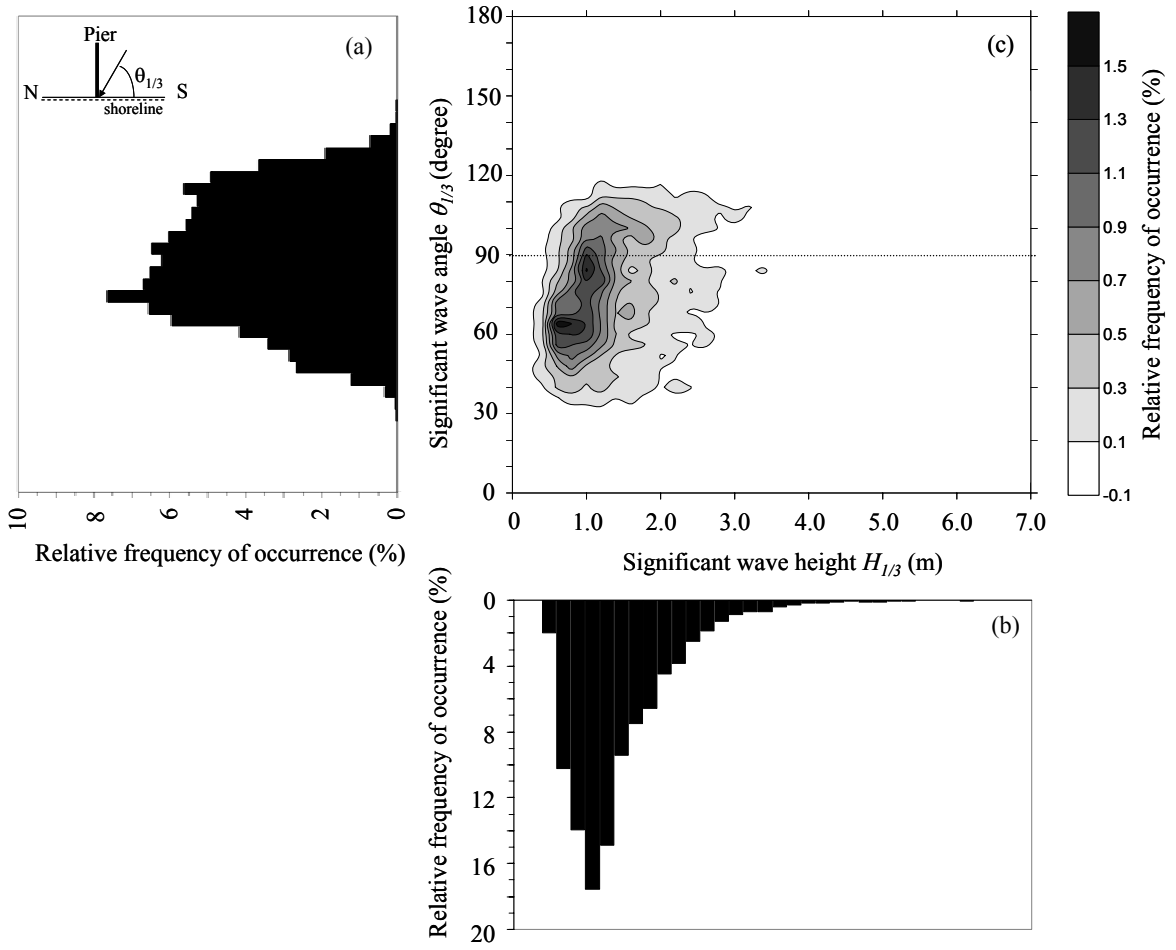

Figure 20: Frequency of occurrence histogram of (a) $\theta_{1/3}$, (b) $H_{1/3}$, and (c) their combination observed in 2005 and 2006.

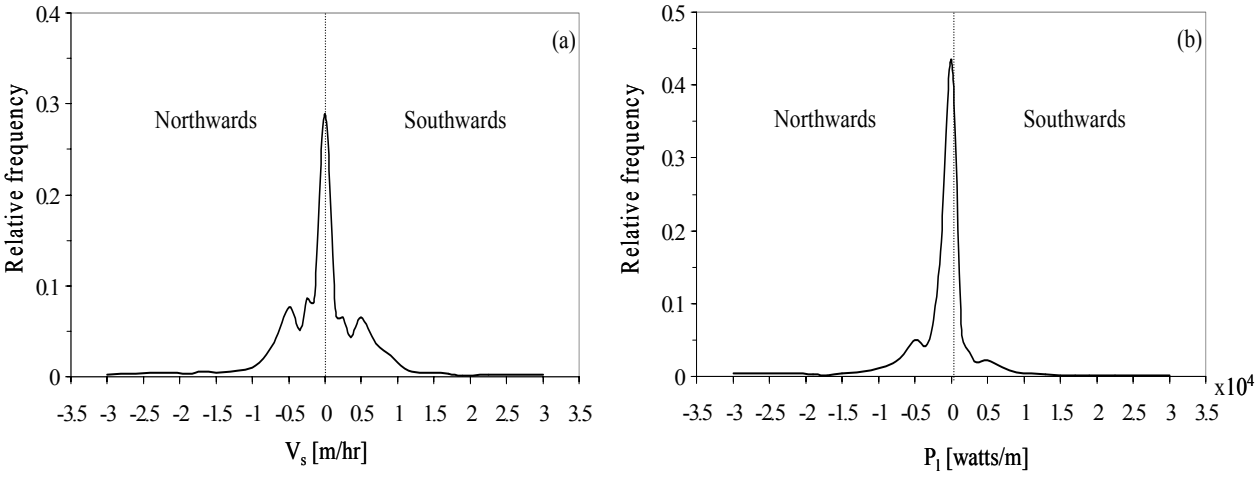

Figure 21: Frequency histogram of (a) V_s, and (b) P_l observed in 2005 and 2006

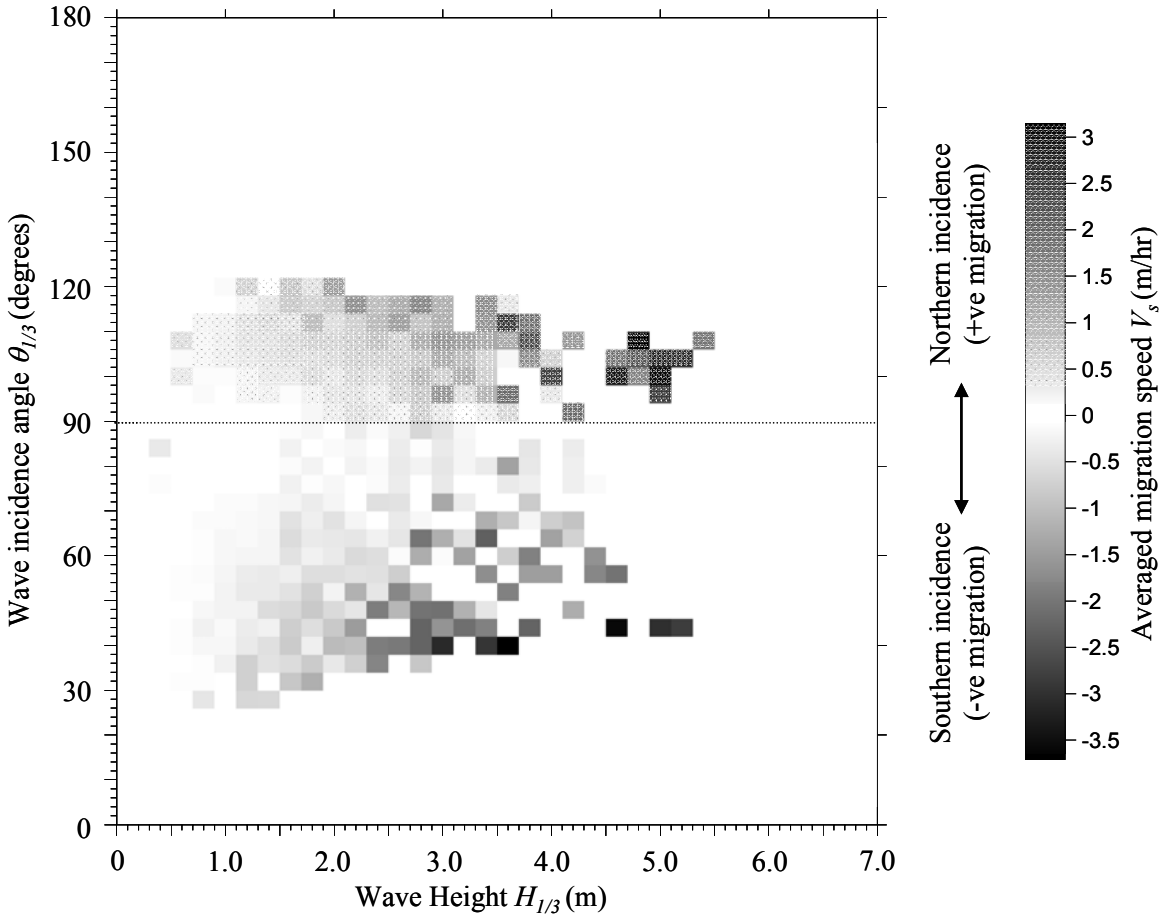

Figure 22: Relationship between migration speeds $V_{s,}$ and $H_{1/3}$ and $\theta_{1/3}$ for the observations of 2005 and 2006.

1